Atmos. Chem. Phys. Discuss., 11, 11861–11909, 2011
www.atmos-chem-phys-discuss.net/11/11861/2011/
doi:10.5194/acpd-11-11861-2011

Atmospheric Chemistry and Physics Discussions

Lidar-derived PM_{10} and comparison with regional modeling in the frame of the MEGAPOLI Paris summer campaign

P. Royer[1,2], P. Chazette[1], K.S artelet[3], Q. J. Zhang[4,5], M. Beekmann[4], and J.-C. Raut[6]

[1]Laboratoire des Sciences du Climat et de l'Environnement (LSCE), Laboratoire mixte CEA-CNRS-UVSQ, UMR 1572, CEA Saclay, 91191 Gif-sur-Yvette, France
[2]LEOSPHERE, 76 rue de Monceau, 75008 Paris, France
[3]Centre d'Enseignement et de Recherche en Environnement Atmosphérique (CEREA), Joint Laboratory Ecole des Ponts Paris Tech/EDF R&D, Université Paris-Est, 6–8 Avenue Blaise Pascal, Cité Descartes Champs-sur-Marne, 77455 Marne la Vallée, France
[4]Laboratoire Inter-universitaire des Systèmes Atmosphériques (LISA), Laboratoire mixte Paris VII-UPEC-CNRS, UMR 7583, 61 Avenue du Général de Gaulle, 94010 Créteil, France
[5]ARIA Technologies, 8-10 rue de la ferme, 92100, Boulogne-Billancourt, France
[6]Laboratoire Atmosphères Milieux Observations Spatiales (LATMOS), Laboratoire mixte UPMC-UVSQ-CNRS, UMR 8190, Université Paris 6, 4 Place Jussieu, 75252 Paris, France

Received: 8 March 2011 – Accepted: 7 April 2011 – Published: 15 April 2011

Correspondence to: P. Royer (philippe.royer@lsce.ipsl.fr)

Published by Copernicus Publications on behalf of the European Geosciences Union.

Abstract

An original approach using mobile lidar measurements was implemented to validate mass concentrations (PM_{10}) predicted by chemistry-transport models. A ground-based mobile lidar (GBML) was deployed around Paris onboard a van during the MEGAPOLI (Megacities: Emissions, urban, regional and Global Atmospheric POLlution and climate effects, and Integrated tools for assessment and mitigation) summer experiment in July 2009. The measurements performed with this Rayleigh-Mie lidar are converted into PM_{10} profiles using optical-to-mass relationships previously established from in situ measurements performed around Paris for urban and peri-urban aerosols. The method is described here and applied to the 10 measurements days (MD). MD of 1, 15, 16 and 26 July 2009 correspond to contrasted levels of pollution and atmospheric conditions. They are analyzed here in more details. Lidar-derived PM_{10} are compared with results of simulations from POLYPHEMUS and CHIMERE chemistry-transport models (CTM) and with ground-based observations from AIRPARIF network. GBML-derived and AIRPARIF in situ measurements have been found to be in good agreement with a mean Root Mean Square Error RMSE (and a Mean Absolute Percentage Error MAPE) of 5.9 $\mu g\,m^{-3}$(21.0%) with peri-urban and 8.7 $\mu g\,m^{-3}$ (25.4%) with urban relationships, respectively. The comparisons between CTMs and lidar have shown that CTMs tend to underestimate wet PM_{10} concentrations as revealed by the mean wet PM_{10} observed during the 10 MD of 22.7, 20.0 and 17.5 $\mu g\,m^{-3}$ for lidar with peri-urban relationship, POLYPHEMUS and CHIMERE models, respectively. This leads to a RMSE (and a MAPE) of 7.2 $\mu g\,m^{-3}$ (33.4%) and 7.4 $\mu g\,m^{-3}$ (32.0%) when considering POLYPHEMUS and CHIMERE CTMs, respectively. Wet integrated PM_{10} computed (between the ground and 1 km above the ground level) from lidar, POLYPHEMUS and CHIMERE results have been compared and have shown similar results with a RMSE (and MAPE) of 6.7 $\mu g\,m^{-2}$ (30.7%) and 7.1 $\mu g\,m^{-2}$ (28.4%) with POLYPHEMUS and CHIMERE when comparing with lidar-periu-urban parametrization. The values are of the same order of magnitude than other comparisons realized in previous studies. The discrepancies

ACPD

11, 11861–11909, 2011

observed between models and measured PM_{10} can be explained by difficulties to accurately model the background conditions, the positions and strengths of the plume, the vertical diffusion (as well as the limited vertical model resolutions) and the chemical modeling such as the formation of secondary aerosols.

1 Introduction

Aerosol pollution studies in urban centers are of increasing interest as they directly concerns almost half of the world's population. Moreover, urban population is expected to continue to increase during the next decades. Epidemiological studies have clearly established that small particles with an aerodynamic diameter below 2.5 µm ($PM_{2.5}$) and below 1 µm (PM_1), and mainly originating from traffic and industrial activities, have an impact on human health by penetrating the respiratory system and leading to respiratory (allergies, asthma, altered lung function) and cardiovascular diseases (e.g. Dockery and Pope, 1996; Lauwerys, 1982). The study of air quality in megacities, with often large particulate matter loads, and potentially large health impact is thus an important issue (e.g. Gurjar et al., 2008). In particular, it is still important to improve our understanding of physic-chemical, transport and emission processes that play a key role in formation of pollution peaks within megacities and their surroundings. In addition, several studies have also shown that megacities have an important regional impact on air quality and climate (e.g. Lawrence et al., 2007).

The Paris agglomeration with about12 millions of inhabitants is one of the three megacities in Europe (with London and Moscow). Air quality is continuously monitored over the agglomeration by a dedicated surface network (AIRPARIF, http://www.airparif.asso.fr/). Furthermore, aerosol chemical and optical properties over Paris have been investigated in the framework of several campaigns: ESQUIF in 1999 (Etude et Simulation de la QUalité de l'air en Ile de France; Vautard et al.; 2003; Chazette et al., 2005), MEAUVE (Modélisation des Effets des Aérosols en Ultra Violet et Expérimentation) in 2001 (Lavigne et al., 2005), LISAIR (Lidar pour la Surveillance de l'AIR) in 2005 (Raut and Chazette, 2007) and ParisFog in 2007 (Elias et al., 2009; Haeffelin et al.,

ACPD
11, 11861–11909, 2011

2010). Ground-based in-situ measurements in dry conditions performed during these campaigns gave the opportunity to determine optical-to-mass relationships for urban, peri-urban and rural environments over the Ile-de-France region (with Paris in its center) (Raut and Chazette, 2009).

In the frame of the FP7/MEGAPOLI project (seventh Framework Programme/Megacities: Emissions, urban, regional and Global Atmospheric POLlution and climate effects, and Integrated tools for assessment and mitigation; http://megapoli.dmi.dk/), an intensive campaign was organized in the Ile de France region in summer (July) 2009 and winter (15 January–15 February) 2010, in order to better quantify organic aerosol sources in a large megacity in temperate latitudes. A large ensemble of ground based measurements at three primary and several secondary sites, by mobile vans, and by aircraft has been set-up. Detailed measurements of aerosol chemical composition and physico-chemical properties, of gas phase chemistry and of meteorological variables were performed on these platforms. Campaign objectives and measurement set-up will be described in detail in a later paper in this special section. As part of this campaign, a ground-based mobile lidar (GBML) was deployed onboard a van in order to investigate the aerosol load and the evolution of aerosol optical properties in the urban plume.

We present here vertically-resolved PM_{10} (mass concentration of aerosols with an aerodynamic diameter lower than 10 µm) retrieved from GBML measurements performed during the MEGAPOLI campaign using optical-to-mass relationships previously established over the Paris region. In addition, a comparison with two regional chemical-transport models is performed. The next section (Sect. 2) details the experimental setup (instrumentation and observation strategy). The modeling approach is detailed in Sect. 3 as well as the commonalities and differences between the two CTMs. The methodology, uncertainties and results of lidar-derived PM_{10} are presented in Sect. 4 and compared to AIRPARIF measurements. Finally, CHIMERE and POLYPHEMUS CTMs simulations are compared to GBML-derived and AIRAPARIF-measured PM_{10} (Sect. 5).

ACPD
11, 11861–11909, 2011

2 Experimental setup

2.1 Instrumentation

2.1.1 Ground-based mobile lidar

Ground based mobile lidar (GBML) used during the MEGAPOLI campaign is based on an ALS450® lidar commercialized by LEOSPHERE company and initially developed by the Commissariat à l'Energie Atomique (CEA) and the Centre National de la Recherche Scientifique (CNRS) (Chazette et al., 2007). The main characteristics of this lidar are summarized in Table 1. The acquisition is realized with a PCI eXtensions for Instrumentation (PXI®) system at 100 MHz (National Instruments). It is based on an Ultra® Nd:Yag laser manufactured by Quantel company, delivering ~6 ns width pulses at the repetition rate of 20 Hz with a mean pulse energy of 16 mJ at 355 nm. This compact (~65 × 35 × 18 cm^3) and light (~40 kg for the lidar head and electronics) instrument was taken onboard a van with a power supply delivered by 4 batteries (12 V, 75A/h) giving an autonomy of ~3 h30 min. This system is particularly well-adapted to air pollution and tropospheric aerosol study thanks to its full overlap reached at about 150–200 m and its high vertical resolution of 1.5 m (15 m after filtering). The detection is realized with photomultiplier tubes and narrowband filters with a bandwidth of 0.3 nm. It gives access to the aerosol optical properties (depolarization ratio and extinction coefficient in synergy with sun-photometer measurements) and the atmospheric structures (planetary boundary layer (PBL) and residual heights, aerosol and cloud layers) with a temporal resolution of 20 s.

2.1.2 AIRPARIF network

AIRPARIF is the regional operational network in charge of air quality survey around Paris area. It is composed of 68 stations spread out in a radius of 100 km around Paris measuring every hour critical gases and/or aerosol concentrations (PM_{10} and $PM_{2.5}$).

ACPD
11, 11861–11909, 2011

Two different types of stations are distinguished: 26 stations close to the traffic sources and 42 background (urban, peri-urban or rural) stations. From the entire set of measurements (NO, NO_2, ozone, PM_{10}, other pollutants, depending on the site), we have only used here PM_{10} concentrations measurements performed with automatic TEOM instruments (Tapered Element Oscillating Microbalance, Pataschnik and Rupprecht, 1991). PM_{10} concentrations are regulated in France. Since 2005 the threshold values are 40 $\mu g\,m^{-3}$ as an annual average and 50 $\mu g\,m^{-3}$ as a daily average which must not to be exceeded has on more than 35 days per year. The advice and alert thresholds are respectively 80 and 125 $\mu g\,m^{-3}$ in daily mean. The uncertainty on PM_{10} concentrations measured with TEOM instrument has been assessed to be between 14.8 and 20.9% (personal communication from AIRPARIF). It is noteworthy that TEOM measurements correspond to dry PM_{10} as sampling is performed through a warmed inlet at ~50 °C.

Figure 1 shows the localization of the 22 AIRPARIF stations measuring PM_{10} concentrations: 10 urban (green circles), 3 peri-urban (blue circles), 3 rural (cyan circles) and 6 traffic stations (red circles) according to AIRPARIF criteria. These latter are not considered in this study because they are not representative of background aerosol concentrations.

2.1.3 AERONET sun-photometer network

The AErosol RObotic NETwork (AERONET) is an automatic and global network of sun-photometers which provides long-term and continuous monitoring of aerosol optical, microphysical and radiative properties (http://aeronet.gsfc.nasa.gov/, Holben et al., 1998). Each site is composed of a 318A® sun and sky scanning spectral radiometer manufactured by CIMEL Electronique. For direct sun measurement eight spectral bands are used between 340 and 1020 nm. The five standard wavelengths are 440, 670, 870, 940 and 1020 nm. Aerosol Optical Depth (AOD) values are computed for three data quality levels: level 1.0 (unscreened), level 1.5 (cloud-screened), and level 2.0 (cloud screened and quality-assured). The total uncertainty on AOD is $< \pm 0.01$ for

ACPD
11, 11861–11909, 2011

$\lambda > 440$ nm and $< \pm 0.02$ for $\lambda < 440$ nm (Holben et al., 1998). Four AERONET sun-photometers are located within the Ile-de–France region inside Paris area at Paris intramuros, Palaiseau, Créteil and Fontainebleau sites. We only used in this study level 2.0 AOD data at 340, 380 and 440 nm from Paris (latitude 48.85° N; longitude 2.36° E; altitude 50 m) and Palaiseau (latitude 48.72° N; longitude 2.21° E; altitude 156 m) sun-photometers stations (see yellow triangles on Fig. 1) which were available during MEGAPOLI campaign.

2.2 Lidar-van travelling patterns

2.2.1 Description and rationale

During the MEGAPOLI summer campaign GBML was used to perform measurements along and across the pollution plume emitted by Paris and its suburbs. The main goal was to determine the atmospheric structures (PBL height, cloud and aerosol layers) and the evolution of the aerosol optical properties (aerosol extinction coefficient and depolarization ratio) during its transport from the agglomeration to about 100 km downwind. Aerosol optical properties are indeed functions of the aging and hygroscopic processes acting on pollution particles (Randriamiarisoa et al., 2006). The lidar measurements were triggered based on chemical forecasts delivered by the PREV'AIR system (Rouil et al., 2009; Honoré et al., 2008, www.prevair.org), and which were especially processed for the campaign, for days when the occurrence of a pollution plume downwind of Paris could be expected (light winds in general below about 5 m s^{-1} at 500 m height, cloud free or partially cloudy conditions). Examples of lidar-van circuits are shown in decimal hours (Local Time LT) on Fig. 2 for 1 (2a), 15 (2b), 16 (2c) and 26 July 2009 (2d), for the main representative cases. GBML measurements were performed either following the pollution plume (1, 15, 16 20, 21, 28 and 29 July 2009) or by circling in the suburbs of Paris at ~25 km from downtown (for 2, 4 or 26 July 2009). The circular tracks were performed when the meteorological forecasts gave horizontal wind fields not suited for a well-defined pollution plume formation, mainly in the case of a horizontal with a mean velocity lower than 4–5 m s^{-1}.

ACPD
11, 11861–11909, 2011

2.2.2 Meteorological condition and representativity of the spatiotemporal sampling

Table 2 summarizes meteorological conditions (wind direction and velocity, relative humidity RH, maximum surface temperature), levels of pollution, AOD and extinction-to-backscatter values (so-called Lidar Ratio LR) at 355 nm observed during the 10 measurements days (MD) involving GBML in cloud-free condition. Wind directions and velocity at ∼250 m are obtained from the Mesoscale Model MM5 and maximum temperatures from in situ ground-based measurements, RH from radiosoundings at 12:00 h (in Universal Time UT) at Trappes (about 30 km in the South-west of the Paris town center) and pollution levels from AIRPARIF urban background stations. AOD (± its standard deviation) at 355 nm is computed with AOD at 380 nm from Palaiseau AERONET sunphotometer station using the Angstrom exponent (Angstrom, 1964) between 340 and 440 nm.

The representativeness of air masses origin observed during the MEGAPOLI summer campaign has been evaluated by comparing with 3-day HYSPLIT (HYbreid Single Particle Lagrangian Integrated Trajectory Model) backward trajectories (http://ready.arl.noaa.gov/HYSPLIT.php) ending at 500 m above ground level (a.g.l.) for the month of July between 2005 and 2010 (Table 3) using 1° × 1° winds from Global Data Assimilation System (GDAS). The origin of air masses for July 2009 is in good agreement with the mean of 2005–2010 where most of the air masses came from south-western (20% for 2005–2010 and 21% for July 2009) and western sectors (41% for 2005–2010 and 60% for July 2009). If we now consider only MD in July 2009 the distribution is significantly different with most air masses observed from the south-western sector (40%) and an important contribution of the southern sector (20%) whereas the western sector only represents 20%. In fact, MD have only been realized in good weather conditions, which can explain that the southern sector is over represented and the western sector under represented.

ACPD
11, 11861–11909, 2011

3 Modeling approach

Two Chemistry-transport models (CTM) have been applied to simulate PM_{10} on each MD previously presented. The main characteristics of the two CTMs used in the simulations are summarized in Table 4.

3.1 POLYPHEMUS platform

The POLYPHEMUS air-quality modeling plateform (http://cerea.enpc.fr/polyphemus) is used with the CTM model Polair3D, the gaseous chemistry scheme Regional Atmospheric Chemistry Model (RACM, Stockwell et al., 1997), and the aerosol model SIREAM-AEC (Kim et al., 2011a; Debry et al., 2007; Pun et al., 2002). Polyphemus/Polair3D has already been used for many applications, such as by Sartelet et al. (2007a, 2008), Roustan et al. (2010), Kim et al. (2011b) at the continental scale, Tombette and Sportisse (2007), Sartelet et al. (2007b), Tombette et al. (2008), Roustan et al. (2011) at the urban/regional scale. Three nested simulations are performed here: Europe, France and Greater Paris. The horizontal domain is (35–70° N; 15° W–35° E) with a resolution of 0.5° × 0.5° over Europe, (41–52° N; 5° W–10° E) with a resolution of 0.1° × 0.1° over France and (47.9–50.1° N; 1.2° W–3.5° E) with a resolution of 0.02° × 0.02° over Greater Paris. Over Europe, the horizontal resolution is the same as in Sartelet et al. (2007a), while it is finer than in Tombette and Sportisse (2005) over Greater Paris: 0.02° against 0.05°. Results of the simulation over Paris are used for the comparison to lidar data. In all simulations, 9 vertical levels are considered from the ground to 12 kilometers. Concerning the land use coverage, the Global Land Cover Facility (GLCF2000) map with 23 categories is used. The meteorological data are obtained from the 5th Penn State MM5 model (Dudhia, 1993), version 3.6, with a horizontal resolution of 36 km. Biogenic emissions are computed as in Simpson (1999). Over Europe and France, the European Monitoring and Evaluation Program (EMEP, http://www.emep.int/) expert inventory for 2005 is used. Over Greater Paris, anthropogenic emissions are generated with the AIRPARIF inventory for 2000 where available

ACPD
11, 11861–11909, 2011

and with the EMEP expert inventory for 2005 elsewhere. More details on the model description and on the use of AIRPARIF and EMEP inventories may be found in Sartelet et al. (2007a) and Tombette and Sportisse (2007) respectively. Further details on the options used in the modeling are given in Table 4.

3.2 CHIMERE model

The second model used here is the eulerian regional chemistry-transport model CHIMERE in its version V2008B (see http://www.lmd.polytechnique.fr/chimere/ for a detailed documentation). The model has been largely applied for continental scale air quality forecast (Honoré et al., 2008; http://www.prevair.org), for sensitivity studies, for example with respect to chemical regimes (Beekmann and Vautard, 2010), and for inverse emission modeling (Konovalov et al., 2006). The model has also been extensively used to simulate photooxidant pollution build-up over the Paris region (e.g., Vautard et al., 2001; Beekmann et al., 2003; Derognat et al., 2003; Deguillaume et al., 2007, 2008), and on several occasions to simulate particulate matter levels over the region (e.g. Bessagnet et al., 2005; Hodzic et al., 2005; Sciare et al., 2010). The initial gas phase chemistry only model has been described by Schmidt et al. (2001) and Vautard et al. (2001), the aerosol modules by Bessagnet et al. (2004, 2008).

The aerosol module includes primary organic (POA) and black carbon (BC), other unspecified primary anthropogenic particulate matter (PM) emissions, wind-blown dust, sea salt, secondary inorganics (sulfate, nitrate and ammonium) as well as secondary organic aerosols (SOA) from anthropogenic and biogenic origin, and particulate water. A sectional size distribution over 8 size bins, geometrically spaced from 40 nm to 10 µm in physical diameter, is chosen. The thermodynamic partitioning of the inorganic mixture (i.e. sulfate, nitrate, and ammonium) is computed using the ISORROPIA model (Nenes et al., 1998, http://nenes.eas.gatech.edu/ISORROPIA), which predicts also the water content. SOA formation of anthropogenic and biogenic origin is predicted by the Pun et al. (2006) scheme, with adaptations described in Bessagnet et al. (2008). The dynamical processes influencing aerosol growth such as nucleation,

ACPD
11, 11861–11909, 2011

coagulation and absorption of semi-volatile species are included in the model as described in Bessagnet et al. (2004). In this work, the model is set up on two nested grids: a continental domain (35–57.5° N ; 10.5° W–22.5° E) with 0.5° resolution, and a more refined urban/regional domain covering the Ile-de-France and neighboring regions (47.45–50.66° N; 0.35° W–4.41° E) with approximately a 3 km horizontal resolution. In the vertical, eight hybrid-sigma vertical layers extend up to 500 hPa, the first layer going up to about 40 m. Meteorological input is provided by Penn State University (PSU) National Center for Atmospheric Research (NCAR) MM5 model (Dudhia, 1993) which is run here with two nested grids covering the European domain with a 45 km horizontal resolution and North-Western Europe with a 15 km resolution. MM5 is forced by the National Centers for Environmental Prediction (NCEP) Global Forecast System (GFS) final (FNL) data. Anthropogenic gaseous and particulate emissions are derived from EMEP annual totals (http://www.ceip.at/emission-data-webdab/). For the nested Ile-de-France grid, refined emissions are used as in Sciare et al. (2010), elaborated by the 6 partners of the EtudeS Multi RégionALes De l'Atmosphère (ESMERALDA) project (AIRPARIF, AIR NORMAND, ATMO PICARDIE, ATMO CHAMPAGNE-ARDENNE, ATMO NORD PAS-DE-CALAIS and LIG'AIR). Biogenic emissions are calculated from the Model of Emissions of Gases and Aerosols from Nature (MEGAN) data base (Guenther et al., 2006). LMDz-INCA (Laboratoire de Météorologie Dynamique zoom – INteractions avec la Chimie et les Aérosols) monthly mean concentrations are used as boundary conditions for gases and aerosols (Hauglustaine et al., 2004).

4 Lidar-derived PM_{10} concentrations

4.1 Aerosol extinction coefficient derived from GBML measurements

The first step before the assessment of the aerosol mass concentration is to derive the aerosol extinction coefficient from the lidar profiles. Such an inversion procedure

ACPD
11, 11861–11909, 2011

requires the knowledge of the lidar ratio (LR) and has been well discussed in several previous studies where uncertainty sources are exhaustively quantified (e.g. Chazette, 2003; Raut et Chazette, 2009a; Royer et al., 2010). The height-independent LR values (Table 2) are determined using a Klett algorithm (Klett, 1985) and a dichotomous approach on LR values converging until the difference between lidar and AERONET sunphotometer AOD at 355 nm is below 0.02 (Chazette, 2003). The values are reported on Table 2 with their standard deviations. That latter includes the temporal variability and mainly the error associated to both the lidar signal to noise ratio and the uncertainty on the sunphotometer-derived AOD. On 1, 2 and 16 July, 2009, an additional N_2-Raman lidar (NRL) was operational and LR has been derived within the mixed layer independently of the sunphotometer measurements as in Royer et al. (2010). Values of 54.4, 56.1 and 34.9 sr have been retrieved for those three days, respectively. The NRL-derived mean LR is in good agreement with that retrieved from the synergy between GBML and sunphotometer with a discrepancy of ~3 sr. On 15, 21 and 29 July 2009, when cloudy conditions prevented from retrieving LR values using the sunphotometers, climatologic LR values have been used for the lidar inversion. On 15 July 2009, when a mixing of pollution and dust aerosols was observed, a LR of 50 sr was chosen (e.g. 57 sr measured with Raman lidar at 355 nm in Greece in Giannakaki et al., 2010). On 21 July 2009 dust layers have also been observed over the PBL by lidar measurements but did not penetrate into it. For this day the LR has been taken to 90 sr in the PBL (value observed for pollution aerosols in the Paris area; Chazette et al., 2005; Raut and Chazette, 2007) and 40 sr in the dust aerosol layer (e.g. 37 sr in Giannakaki et al., 2010, 45 in Royer et al., 2010 with Raman lidars at 355 nm). On 29 July 2009 where only pollution aerosols are observed we used a LR of 90 sr.

The 10 MD involving the mobile lidar have been inverted into extinction coefficient profiles using a Klett algorithm (Klett, 1985) with the mean LR values determined as described above (see values in Table 2).

ACPD
11, 11861–11909, 2011

4.2 Method and optical-to-mass relationships

The method to retrieve PM_{10} concentrations from lidar measurements has been first applied to aerosol observed in an underground railway station of Paris (Raut et al., 2009a, b). Wet PM_{10} concentrations in PBL have been inferred from lidar aerosol extinction coefficient ($\alpha_{ext,355}$) using a similar empirical optical-to-mass relationship between measurements from nephelometer and TEOM instruments (Raut and Chazette, 2009):

$$PM_{10,wet} = \underbrace{C_0 \cdot \varpi_{0,355} \cdot \left(\frac{700}{355}\right)^{-a}}_{1/s_{ext,\,355}} \alpha_{ext,\,355} \quad (1)$$

where $s_{ext,\,355}$ is the specific extinction cross-section at 355 nm, $\varpi_{0,355}$ is the single-scattering albedo at 355 nm and a the Angström exponent between 450 and 700 nm which is assumed to be the same as the Angström exponent between 355 and 700 nm. C_0 is the slope of regression analysis between the nephelometer scattering coefficients at 700 nm and the TEOM PM_{10} measurements performed simultaneously during several campaigns in Paris and its suburbs. Raut and Chazette (2009b) have determined different values of C_0, $\varpi_{0,355}$, a and $s_{ext,355}$ for dust, urban, peri-urban, rural aerosol types (see Table 5). Urban relationship has been determined from in-situ measurements in the center of Paris during ESQUIF (Chazette et al., 2005) and LISAIR (Raut and Chazette, 2007) campaigns, respectively in 1999 and 2005. Peri-urban situations have been identified during ParisFog in 2007 (Elias et al., 2009) and ESQUIF campaign data. They correspond to measurements directly influenced by urban sources. Rural conditions influenced by pollution in the Paris area have been encountered during the MEAUVE campaign in 2001 (Lavigne et al., 2005). For the comparisons with AIRPARIF and CTMs simulations, the urban parametrization will be used for lidar observations inside the pollution plume in the inner suburbs of Paris, peri-urban relationship for measurements outside the pollution plume in the inner suburbs and measurements inside

ACPD
11, 11861–11909, 2011

the plume far from Paris. Rural relationship will be applied for observations far from Paris center outside the pollution plume. A combination of dust and pollution aerosol specific extinction cross-sections is used on 15 July 2009 where a mixing of dust and pollution aerosols is observed. The different sources of uncertainties on the retrieval of PM_{10} from lidar measurements are discussed in the following section.

4.3 Uncertainties on PM_{10}

The retrieval of PM_{10} from lidar measurements is affected by uncertainties in the measurements: extinction coefficient profiles and specific extinction cross-sections at 355 nm, as well as uncertainties linked to the aerosol type assumption (urban, peri-urban, rural or dust). Lidar measurements are inverted into extinction coefficient profiles using a Klett algorithm with the mean LR value in Table 2. Considering an uncertainty of 0.02 (Holben et al., 1998) on *AOD* sun-photometer constraint, the total relative uncertainty on the extinction coefficient profile is 21%, 13% and 8% for a mean AOD of 0.1, 0.2 and 0.5 at 355 nm, respectively (Royer et al., 2010). These calculations take into account (1) the uncertainty on the a priori knowledge of the vertical profile of the molecular backscatter coefficient as determined from ancillary data, (2) the uncertainty of the lidar signal in the altitude range used for the normalization, (3) the statistical fluctuations in the measured signal, associated with random detection processes and (4) the uncertainty on AOD sun-photometer constraint.

Uncertainties in the specific extinction cross-sections have been assessed as 12% (resp. 26%) for urban and peri-urban (resp. dust and rural) relationships taking into account uncertainties on C_0, $\omega_{0,355}$ and a (Raut and Chazette, 2009).

Only uncertainties linked to the measurements are quantified here. Concerning the aerosol type assumption, uncertainties are linked to the empirical optical-to-mass relationship, which assumes a particulate chemical composition and granulometry for each aerosol type. Taking a peri-urban relationship instead of an urban (resp. rural) relationship leads to an underestimation (resp. overestimation) of PM_{10} concentration of 30% (resp. 20%).

ACPD
11, 11861–11909, 2011

The influence of hygroscopicity has been neglected for the comparisons with AIRPARIF dry PM_{10} since RH values observed (see Table 2) during the 10 MD stay below 49% at 200 m. The liquid water content of particles computed from ISOROPIA (Nenes et al., 1998) using the particulate composition of POLYPHEMUS (see Sect. 4) along the lidar trajectories indicates that water represents in average 25.5% on 1 July, 20.4% on 2 July, 14.4% on 4 July, 6.7% on 15 July, 12.7% on 16 July, 12.3% on 20 July, 12.7% on 21 July, 5.4 on 26 July, 11.3% on 28 July and 10.0% on 29 July of dry modeled PM_{10} concentrations.

Assuming the different sources of uncertainties to be independent leads to an overall relative uncertainty on the measurements of 24%, 17% and 13% for peri-urban and urban relationships considering a mean AOD of 0.1, 0.2 and 0.3, respectively (see values Table 5). For rural and dust aerosols the total uncertainty on PM_{10} are higher (33%, 28% and 26%) due to higher uncertainties of 26% on specific extinction cross-sections. The expected uncertainties in lidar PM_{10} are then been computed in Table 6 for rural, peri-urban and urban relationships using sun-photometer AOD values observed during each MD. They range from 13 to 21 l (resp. 27 to 31%) with a mean value of 17% (resp. 29%) for peri-urban and urban (resp. rural and dust) relationships.

4.4 Comparison between GBML-derived PM_{10} and AIRPARIF measurements

Figures 3 and 4 show the spatial distributions of wet PM_{10} at ~250 m a.g.l. (where the lidar overlap function reaches 1) on 1 (Fig. 3a), 15 (Fig. 3b), 16 (Fig. 4a) and 26 (Fig. 4b) July 2009. Lidar-derived and AIRPARIF ground-based PM_{10} are shown in the left column. Winds at ~250 m a.g.l. used in POLYPHEMUS and CHIMERE simulations are also indicated with black arrows to highlight the direction of the pollution plume for each model.

Comparisons between lidar and AIRPARIF PM_{10} have been expressed for each relationship (urban, peri-urban and rural) in terms of Root Mean Square Error (RMSE) and Mean Absolute Percentage Error (MAPE) given by the following equation:

ACPD
11, 11861–11909, 2011

$$\mathrm{RMSE} = \sqrt{\frac{1}{n}\sum_{i=1}^{n}(\mathrm{PM}_{10}^{\mathrm{mod}} - \mathrm{PM}_{10}^{\mathrm{mes}})^2} \quad (2)$$

$$\mathrm{MAPE} = \frac{1}{n}\sum_{i=1}^{n}\frac{\left|\mathrm{PM}_{10}^{\mathrm{mod}} - \mathrm{PM}_{10}^{\mathrm{mes}}\right|}{\left(\frac{\mathrm{PM}_{10}^{\mathrm{mod}} + \mathrm{PM}_{10}^{\mathrm{mes}}}{2}\right)} \quad (3)$$

where n is the number of observations and, $\mathrm{PM}_{10}^{\mathrm{mod}}$ and $\mathrm{PM}_{10}^{\mathrm{mes}}$ are the modeled and measured PM_{10}, respectively. RMSE and MAPE are both summarized in Table 6. Only AIRPARIF stations located at less than 10 km from GBML are considered for the comparisons.

The 1 July 2009 (Fig. 3a) is characterized by high surface temperatures (up to 30 °C) and anticyclonic conditions. Lidar measurements are performed leeward inside the pollution plume in the southwest of Paris from Saclay (latitude 48.73° N; longitude 2.17° E) to Chateaudun (latitude 48.1° N; longitude 1.34° E) between 12:48 and 15:58 LT. It is the most polluted day of the campaign with high levels of pollutions and averaged PM_{10} of $43 \pm 18\,\mu\mathrm{g\,m^{-3}}$ obtained with the peri-urban relationship at 210 m height along the GBML van-circuit and between 40 and $80\,\mu\mathrm{g\,m^{-3}}$ measured by AIRPARIF background stations. Only peri-urban and rural relationships have to be considered for this MD as measurements have been realized far from the sources inside and outside the pollution plume. The highest values of GBML-derived PM_{10} (70–$90\,\mu\mathrm{g\,m^{-3}}$ for peri-urban relationship) are observed at the beginning of the track, in agreement with the values measured at 13:00 h LT by AIRPARIF at Issy-les-Moulineaux ($66\,\mu\mathrm{g\,m^{-3}}$) and La Défense ($78\,\mu\mathrm{g\,m^{-3}}$) in the southwest of Paris. The decrease of PM_{10} from the center of Paris to its suburb is clearly visible on both AIRPARIF and GBML profiles. GBML-derived PM_{10} decrease down to $50\,\mu\mathrm{g\,m^{-3}}$ with peri-urban relationship near Bois Herpin ($47\,\mu\mathrm{g\,m^{-3}}$ measured by AIRPARIF at 14:00 h LT) and down to $20\,\mu\mathrm{g\,m^{-3}}$ near Chateaudun with the rural parametrization. We can notice the lower concentrations

ACPD
11, 11861–11909, 2011

observed near Saclay at 16:00 h LT than at 13:00 h LT (58 compared with 87 $\mu g\,m^{-3}$ with the peri-urban relationship). This is probably explained by the increase of the PBL height from 1.2 up to 1.8 km leading to a dilution of pollutants as shown in Fig. 4a and b. Note that the increase observed at the top of the PBL is due to a hygroscopic effect, indeed RH increases up to 74% at ~1.1 km in the Trappes radiosounding launched at 12:00 h (UT). A strong thermic convection occurring in the well developed convective mixing layer observed during this day can explain the good correlation observed between PM_{10} at ground and 210 m levels. For this MD, RMSE (MAPE) between GBML and AIRPARIF data is 4.9 and 9.1 $\mu g\,m^{-3}$ (8.1 and 14.8%) using peri-urban and rural relationships.

On 15 July 2009, dust aerosol layers were observed by the lidar measurements as confirmed by the Dust Regional Atmospheric Model (DREAM, http://www.bsc.es/projects/earthscience/DREAM) and the low angstrom exponent close to 0.5 measured by the Palaiseau AERONET sun-photometer. The increase between 08:00 and 09:00 h LT of background PM_{10} and the decrease from 55% to 35% of $PM_{2.5}/PM_{10}$ ratio reported by the AIRPARIF network suggest that dust aerosols have been mixed into the PBL and have reached the surface. At the same time the Palaiseau sun-photometer has measured a slight increase of AOD at 355 nm from 0.16 to 0.19. This increase is used to assess the proportion of dust and pollution extinction specific cross-sections at 355 nm. A climatologic LR of 50 sr corresponding to a mixing of dust and pollution aerosols has been used for the inversion of lidar measurements (e.g. Giannakaki et al., 2010). Figures 3b and 6b show the results of PM_{10} at 210 m along the track. For this MD, lidar measurements have mainly been performed in urban and peri-urban condition. If we only consider pollution aerosols within the PBL, PM_{10} are underestimated compared with AIRPARIF by 9.8 and 13.3 $\mu g\,m^{-3}$ (MAPE of 40.6 and 63.9%) with the urban and peri-urban parametrizations, respectively. Considering a contribution of 54% of dust aerosols in the total PM_{10}, no underestimation is observed and the RMSE is 4.1 and 5.1 $\mu g\,m^{-3}$ (11.4 and 16.3%) with urban and peri-urban relationships. Indeed, this better comparison indicates the presence of a mixed aerosol for this day. On that

ACPD
11, 11861–11909, 2011

day, the mean PM_{10} observed by GBML is $25.7 \pm 2.4\,\mu g\,m^{-3}$ (resp. $22.7 \pm 2.1\,\mu g\,m^{-3}$) with urban (resp. peri-urban) relationships.

On 16 July 2009 (Fig. 5a) GBML measurements are performed in the north of Paris from Saclay (latitude 48.73° N; longitude 2.17° E) to Amiens (latitude 49.89° N; longitude 2.29° E) between 13:00 to 16:30 LT. According to criteria detailed in Sect. 4.2, urban relationships is considered for comparison with AIRPARIF stations located inside the pollution plume (La Défense, Issy-les-Moulineaux and Gennevilliers), peri-urban relationship is considered for measurements far from Paris inside the pollution plume (near Beauvais) and rural relationship for measurements outside the pollution plume near Amiens. Moderate levels of pollutions ($25–35\,\mu g\,m^{-3}$) are observed at Issy-les-Moulineaux, La Défense and Gennevilliers AIRPARIF stations located in the north and the west of Paris, in agreement with GBML-derived PM_{10} ($22–25\,\mu g\,m^{-3}$ for urban). GBML-derived PM_{10} progressively decrease to reach $10\,\mu g\,m^{-3}$ for lidar/rural near Amiens. Only AIRPARIF urban stations under the pollution plume have been compared with lidar measurements. The RMSE (MAPE) is $4.9\,\mu g\,m^{-3}$ (18.5%) with the urban relationship for a mean value of PM_{10} between 19.7 and $25.3\,\mu g\,m^{-3}$ for lidar/peri-urban and lidar/urban, respectively.

On 26 July 2009 a circular lidar-van circuit was realized from 14:40 to 17:30 LT at a distance between 15 and 30 km from Paris center (Fig. 5b). Urban relationship must be considered in the North-Northeast of Paris inside the pollution plume (for the comparisons with Gonesse AIRPARIF stations) and peri-urban relationship for the other stations. With these criteria RMSE is $1.8\,\mu g\,m^{-3}$ and MAPE is 8.1%. Low levels of pollution have been observed (GBML-derived PM_{10} mean value of between 14.2 and $18.2\,\mu g\,m^{-3}$ with peri-urban and urban parametrizations) with background concentration around $13–14\,\mu g\,m^{-3}$ (La Défense, Issy-les-Moulineaux, Vitry-sur-Seine and Lognes AIRPARIF stations) and a slight increase to $17–18\,\mu g\,m^{-3}$ leeward in the north of Paris (Gonesse and Bobigny AIRPARIF stations).

It is noteworthy that PM_{10} measured at Bobigny and Gonesse AIRPARIF stations is particularly high compared with GBLM retrievals especially for southwest wind

ACPD
11, 11861–11909, 2011

directions (15, 21, 28 and 29 July). These stations may be influenced by local emissions from Le Bourget airport located 4–5 km in the southwest of Gonesse and from industrial activities (railway activities) located 0.5–3 km in the southwest of Bobigny. If we exclude these stations, the RMSE between lidar/peri-urban and AIRPARIF decreases from 5.1 to 3 $\mu g\,m^{-3}$ on 15 July, from 11.3 to 5.7 $\mu g\,m^{-3}$ on 21 July and from 8.0 to 3.7 $\mu g\,m^{-3}$ on 28 July.

Considering the 10 MD with all AIRPARIF stations, the mean total RMSE between GBML-derived PM_{10} and AIRPARIF measurements are 5.9 $\mu g\,m^{-3}$ and 8.7 $\mu g\,m^{-3}$ with peri-urban and urban relationships (where most of the comparisons have been realized) and the mean MAPE are 21.0% and 25.4% for mean values of 22.7 ± 3.9 and $30.2 \pm 5\,\mu g\,m^{-3}$, respectively (Table 6). If we exclude Bobigny and Gonesse stations, the RMSE (and MAPE) decrease to 4.5 $\mu g\,m^{-3}$ (17.7%) for lidar/peri-urban and 8.2 $\mu g\,m^{-3}$ (24.6%) for lidar/urban. These discrepancies are in good agreement with the expected uncertainty of 17% computed for urban and peri-urban relationships (see Table 6). Two additional factors have to be taken into account: (1) uncertainties in PM_{10} measured by TEOM instruments (between 15 and 20%, see Sect. 2.1.2) and (2) the possible decorrelation between ground level and PM_{10} values at 210 m a.g.l. Note that significant variations in the aerosol optical signature have been previously observed around Paris by Chazette et al. (2005) and Raut and Chazette (2009) within the first hundred meters above the surface. Thus, differences between lidar derived PM_{10} concentrations and AIRPARIF observations are clearly within the range of expected errors.

5 Comparison with chemistry-transport models

CTM compute concentrations of pollutants at predefined vertical heights. Wet PM_{10} at height levels computed by the CTM have been compared to GBML-derived PM_{10}. At each GBML position and each CTM's vertical height, wet PM_{10} calculated by the CTM are interpolated horizontally and temporally. We present here comparisons at ground and ~200 m a.g.l. The integrated content of PM_{10} derived from both lidar measurements and modeling are also compared to reflect the lidar information within PBL.

ACPD
11, 11861–11909, 2011

5.1 Comparison between lidar and modeling within the low PBL

Figures 3 and 5 show the spatial distribution of wet PM_{10} at ~200 m a.g.l. modeled by POLYPHEMUS and CHIMERE CTMs (central and right panels, respectively) on 1, 15, 16 and 26 July, 2009 at 12:00 h (UT). On Fig. 6 lidar wet PM_{10} measurements estimated with rural (green), peri-urban (orange) and urban (red) relationships is compared with wet PM_{10} modeled along the track with POLYPHEMUS (dark blue) and CHIMERE (light blue) CTMs. Dry PM_{10} at the ground level from AIRPARIF and the lowest model layer of POLYPHEMUS and CHIMERE are also indicated by black, dark blue and light blue filled symbols, respectively.

Most of the comparisons between lidar and models have been realized far from Paris inside the pollution plume or close to Paris outside the pollution plume. We thus consider peri-urban parametrization for these comparisons. Wet PM_{10} between GBML/peri-urban and models have shown the following error statistics in terms of RMSE (MAPE) for POLYPHEMUS and CHIMERE (Table 6): 7.5 (13.4%) and 14.2 $\mu g\,m^{-3}$ (25.1%) on 1 July, 6.6 (31.7%) and 5.0 $\mu g\,m^{-3}$ (21.2%) on 15 July, 4.4 (16.6%) and 6.0 $\mu g\,m^{-3}$ (30.3%) on 16 July and 6.1 (54.3%) and 5.5 $\mu g\,m^{-3}$ (48.5%) on 26 July 2009. Note that on 15 July, the contribution of dust aerosol in the total PM_{10} is found to be 54.2% (12.3 $\mu g\,m^{-3}$) with the lidar/peri-urban, which is in good agreement with CHIMERE (54%). POLYPHEMUS under-estimates the contribution of dust aerosol on that day (26%), because dust aerosol probably comes from long-range transport south of Europe and the boundary conditions used for the European simulation are climatological boundary conditions (they are not specific to July 2009). If we consider all MD, the RMSE (MAPE) between GBML/peri-urban and models PM_{10} are 7.2 (33.4%) and 7.4 $\mu g\,m^{-3}$ (32.0%) for POLYPHEMUS and CHIMERE, respectively. As shown by the mean values for the 10 MD of 22.7, 20.0 and 17.5 $\mu g\,m^{-3}$ for lidar/peri-urban, POLYPHEMUS and CHIMERE models, respectively, both models under-estimate the wet PM_{10} concentrations.

ACPD
11, 11861–11909, 2011

5.2 Comparison between AIRPARIF ground-based measurements and modeling

Dry PM_{10} at the ground level from POLYPHEMUS and CHIMERE CTMs show a systematic underestimation (means of 20.6 and 21.4 $\mu g\,m^{-3}$, respectively) compared to AIRPARIF measurements (27.9 $\mu g\,m^{-3}$). RMSE (MAPE) are 9.1 (32.5%) for POLYPHEMUS and 9.4 $\mu g\,m^{-3}$ (32.8%) for CHIMERE. If AIRPARIF stations in Bobigny and Gonesse are not considered, these values drop to 7.9 $\mu g\,m^{-3}$ (29.2%) for POLYPHEMUS and 8.7 $\mu g\,m^{-3}$ (32.9%) for CHIMERE.

5.3 Comparison between lidar and models in term of integrated PM_{10}

Wet integrated PM_{10} have been computed between the ground level and 1 km a.g.l. for lidar, POLYPHEMUS and CHIMERE models. The top of the PBL has been deliberately excluded to avoid the increase of RH and the formation of clouds in this part of the atmosphere. The results are summarized in Table 7 and two examples of temporal evolution of integrated PM_{10} are given in Fig. 7 for the 1 (7a) and 15 July 2009 (7b). The results are very similar than to is observed when comparing PM_{10} concentrations at ~200 m. All comparisons (see example in Fig. 7) of wet integrated PM_{10} show the same kind of evolution than the one of PM_{10} concentration at 200 m (Fig. 6). However, for the 1 July, the modeled PM_{10} concentrations show less disparities between urban and peri-urban areas than at 200 m, in opposition to the lidar derived PM_{10} concentrations.

Mean integrated PM_{10} are 20.9, 21.1 and 16.2 $\mu g\,m^{-2}$ for GBML/peri-urban, POLYPHEMUS and CHIMERE, respectively. The RMSE (and MAPE) are 6.7 (30.7%) and 7.1 (28.4%) with POLYPHEMUS and CHIMERE when comparing with lidar-periurban parametrization. The fact that results for integrated PM_{10} are very similar to results for PM_{10} concentrations at 200 m suggests that concentrations are well mixed within the boundary layer during the observed periods.

ACPD
11, 11861–11909, 2011

5.4 Comparison to previous studies

The statistical results obtained in this study have been compared to previous regional scale model/measurements comparison studies at the regional scale.

Hodzic et al. (2004) performed a comparison of lidar backscatter signals measured at SIRTA at 600 m a.g.l. during 40 mornings (between 08:00 and 11:00 UT) between October 2002 and April 2003 with the ones derived from CHIMERE simulations. Note that their approach is alternative to our's, in the sense that lidar observables are directly calculated within the model. The relative bias was −25% and the relative RMSE was 38%. The model underestimation was attributed to an underestimation of SOA and mineral dust, the latter not being included in the standard run. These figures are in the range of values obtained in the present study for the CHIMERE model: relative bias −23 % ($-5.2\,\mu g\,m^{-3}$) and relative RMSE of 33% when comparing with lidar with peri-urban relationship. Hodzic et al. (2005) performed a detailed comparison of CHIMERE model simulations with AIRPARIF measurements. In summer (April to September) 2003, the PM_{10} daily mean levels are fairly well predicted, for the ensemble of urban, peri-urban and rural background sites, bias was low ($-2.5\,\mu g\,m^{-3}$),and MAPE was 27%.

Tombette and Sportisse (2007) simulated PM_{10} concentrations over Paris between 1 May 2001 and 30 September 2009 with the POLYPHEMUS system. The comparison of PM_{10} concentrations to AIRPARIF measurements gave similar results to this study (RMSE of $9.5\,\mu g\,m^{-3}$ and MAPE 32%). Roustan et al. (2011) simulated also PM_{10} concentrations over Paris for the year 2005 with the POLYPHEMUS system. The comparison to AIRPARIF measurements led to a similar RMSE ($9.8\,\mu g\,m^{-3}$) as here and as in Tombette and Sportisse (2007). However, PM_{10} concentrations are over-estimated in their study, probably because the measurement network for PM_{10} did not until 2005 measure a large fraction of semi-volatile PM.

The difficulties to accurately model the semi-volatile fraction of PM_{10} at the urban/regional scale is shown by the study of Sartelet et al. (2007b). They compared modeled inorganic components of $PM_{2.5}$ (main part of PM_{10} within urban area) to

ACPD
11, 11861–11909, 2011

measurements over Tokyo for high-pollution episodes. Using the normalized mean bias factor (B_{NMBF}) and the normalized mean absolute error factor (E_{NMAEC}) as statistical indicators, they found that sulfate is well modeled with $|B_{NMBF}| < 25\%$ and $E_{NMAEC} < 35\%$, as suggested as a criterion of model performance by Yu et al. (2006) for sulfate. However, for inorganic semi-volatile components, such as ammonium and nitrate, the model performance was lower with $E_{NMAEC} < 60\%$.

Finally, observations made during the HOVERT campaign (HOrizontal and VERtical Transport of ozone and particulate matter) in the Berlin agglomeration between September 2001 and 2002 were compared to REM3-CALGRID simulations. Relative RMSE differences between observed and simulated urban background PM_{10} was typically around 50% (Beekmann et al., 2007).

As a conclusion of these different studies, statistical model to observation comparison results presented in this study seem in the same order or better than those in previous urban/regional scale studies. The PM_{10} concentrations over Paris were not systematically under-estimated in studies made before 2005, because before 2007 the AIRPARIF measurement network did not measure a large fraction of semi-volatile PM, stressing the importance of an accurate representation of secondary aerosols.

5.5 Factors influencing the PM_{10} modeled concentrations

In order to understand what parameterizations/factors influence the most the aerosols and gas-phase species concentrations, Roustan et al. (2010) performed a sensitivity study over Europe with the POLYPHEMUS system for 2001, by changing one input data set or one parameterization at one time. They did not include the sensitivity to emissions in their study. They found that the modeled PM_{10} concentrations are most sensitive to the parameterization used for vertical turbulent diffusion, and to the number of vertical levels used. Depending on the chemical components of PM_{10} studied, the concentrations are also sensitive to boundary conditions, heterogeneous reactions at the surface of particles, the modeling of aqueous chemistry and gas/particle mass transfer, and deposition for large particles.

ACPD
11, 11861–11909, 2011

Beyond this general model error analysis, it is interesting to try to analyze reasons for actually occurred errors. Differences between simulations and observations may be decomposed into two factors: (1) the background PM_{10} over the domain and (2) the additional build-up from Paris agglomeration. For 26 July, background PM_{10} simulated by both models is lower than the lidar derived one even when using the rural relationship (which gives the lowest values). On the contrary, the superimposed PM_{10} peak due to Paris emissions is well simulated (Fig. 6d).

5.5.1 Influence of transport and boundary conditions

For 16 July, the Paris pollution plume is heading to north north-west as confirmed for example by NO_y measurements on the French Safire ATR-42 aircraft (A. Colomb et al., personal communication, 2011). However, in CHIMERE simulations, the wind is heading to North-north-east, causing a direction shift in the plume. On the contrary, in 1 July, spatial gradients, in particular the shift from large values within and near the agglomeration to much lower ones about 100 km downwind, are qualitatively well depicted by both models. As said above and depicted in Fig. 3a, for this day continental transport from North-East was important and resulted in large PM_{10} values transported to Ile de France, while for the other days, air masses were mainly of maritime origin and much cleaner. This example illustrates that both uncertainties in background PM_{10}, in the position of the plume and in its strength, can affect the PM_{10} concentrations.

5.5.2 Influence of vertical mixing and turbulent diffusion

On 1 July, the low boundary height until midday contributed to the high concentrations observed. Both models represent well the decrease of PM_{10} concentrations at Saclay between 13:00 LT and 16:00 LT, correlated with an increase of the PBL height from 1.2 to 1.8 km. While the Fig. 4 does not show a systematic bias between the simulated and observed boundary layer height (for the example of 1 July), it illustrates that limited vertical model resolution leads to much smoother vertical PM_{10} profiles than those

ACPD
11, 11861–11909, 2011

deduced from lidar, where a sharp transition between the convective boundary layer and free troposphere occurs. This discussion makes evident the strength of this lidar derived data set for model evaluation, because it depicts both horizontal gradients between the agglomeration, the plume, and background values, and vertical gradients between layers affected by pollution sources and not.

5.5.3 Influence of chemical modeling of semi-volatile components

AMS and soot measurements during the MEGAPOLI summer campaign at the Golf site/Livry Gargan at the north-eastern edge of the agglomeration made evident that secondary inorganic aerosol (inorganic and organic) made up about on the average two thirds of PM_{10} aerosol (J. Schneider et al., personal communication, 2011), thus obviously secondary formation processes are important for peri-urban aerosol and will be even more in the plume. Furthermore, the formation of secondary organic aerosol in the urban area and plume is likely to be under-estimated, as made evident in Sciare et al. (2010) for the CHIMERE model for an urban Paris site.

From this error analysis, it becomes clear, that model to observation differences (on the average about 30%) can be in general explained by the combined measurement uncertainties (15–30%) and the minimal simulation uncertainty presented in Roustan et al. (2010) (30% in summer and 20% in winter).

This simulation uncertainty also explains differences between the CHIMERE and Polyphemus simulations. For both models, particular choices of physico-chemical schemes, parameterisations, numerical set-ups and input data have been made, according to Table 4, and consequently result in model to model differences which are coherent with the model uncertainties given above.

ACPD
11, 11861–11909, 2011

6 Conclusions

Ten intensive observation periods (MD) were performed with ground-based mobile Rayleigh-Mie lidar around Paris during the MEGAPOLI summer campaign. Aerosol extinction profiles have been converted into mass concentrations (PM_{10}) profiles using optical-to-mass relationships (urban, peri-urban, rural and dust) previously established for the Paris area. This set of comparisons makes evident horizontal and vertical PM_{10} gradients in air masses within and outside the Paris agglomeration pollution plume and at different distances from the agglomeration. Lidar derived PM_{10} levels are compared with CHIMERE and POLYPHEMUS chemistry-transport models (CTMs) simulations and AIPARIF network ground-based measurements. These comparisons have highlighted a very good agreement between GBML and AIRPARIF network with a RMSE (MAPE) of 5.9 $\mu g\,m^{-3}$ (21.0%) and 8.7 $\mu g\,m^{-3}$ (25.4%) for peri-urban and urban parametrizations (where most of the comparisons have been realized). This value is close to the expected uncertainty of this method. For each MD the pollution plume has been sampled and can be clearly identified from GBML measurements. Lidar measurements give access to the repartition of aerosols mass concentration in the atmospheric column contrarily to in-situ ground-based measurements. The use of a N_2-Raman lidar, measuring aerosol extinction profiles without any assumptions, could significantly improve the retrieval of PM_{10} from ground-based lidar. The comparisons between lidar retrievals and CTMs within the low PBL have shown a RMSE (MAPE) between GBML/peri-urban and models PM_{10} of 7.2 (33.4%) and 7.4 $\mu g\,m^{-3}$ (32.0%) for POLYPHEMUS and CHIMERE models, respectively. Similar differences have been computed for the integrated PM_{10} within the PBL (RMSE of 6.7 $\mu g\,m^{-2}$ (30.7%) and 7.1 $\mu g\,m^{-2}$ (28.4%) for POLYPHEMUS and CHIMERE models, respectively). These differences are partly due to an underestimation of wet PM_{10} as revealed by the mean values for the 10 MD of 22.7, 20.0 and 17.5 $\mu g\,m^{-3}$ for lidar/peri-urban, POLYPHEMUS and CHIMERE models, respectively. When comparing dry PM_{10} at ground level from AIRPARIF ground-based measurements to CTMs simulation RMSE (MAPE) is

ACPD
11, 11861–11909, 2011

9.1 µg m^{-3} (32.5%) with POLYPHEMUS and 9.4 µg m^{-3} (32.8%) with CHIMERE. The discrepancies observed between models and measured PM_{10} can be explained by difficulties to accurately model background conditions, represent model transport (positions and strengths of the plume), limited vertical model resolutions and chemical modeling such as the formation of secondary aerosols. On the whole, model to observation differences are coherent with the error budgets of both observations and simulations and are of the same order of magnitude than comparisons realized in previous studies.

This is one of the first papers presenting results of the MEGAPOLI Paris campaigns. Forthcoming papers will present more detailed results about the comparison of lidar derived PM_{10} measurements with aircraft observations and about model evaluation with chemically resolved aerosol measurements.

Acknowledgements. The research leading to these results has received funding from the European Union's Seventh Framework Programme FP/2007–2011 under grant agreement no. 212520. This work has been supported by the Commissariat à l'Energie Atomique (CEA). The authors would like to thank AIRPARIF and AERONET network for collecting and providing data around Paris used in this study. CHIMERE modelling results have been obtained under Ph-D grant funding by CIFRE (ANRT) attributed to ARIA Technologies and LISA.

The publication of this article is financed by CNRS-INSU.

ACPD
11, 11861–11909, 2011

References

Angström, A.: The parameters of atmospheric turbidity, Tellus, 16, 64–75, 1964.

Aumont, B., Chervier, F., and Laval, S.: Contribution of HONO to the NOx/HOx/O3 chemistry in the polluted boundary layer, Atmos. Environ., 37, 487–498, 2003.

Beekmann M. and Derognat, C.: Monte Carlo Uncertainty analysis of a regional sale transport chemistry model constrained by measurements from the ESQUIF campaign, J. Geophys. Res., 108, 8559, doi:10.1029/2003JD003391, 2003.

Beekmann, M. and Vautard, R.: A modelling study of photochemical regimes over Europe: robustness and variability, Atmos. Chem. Phys., 10, 10067–10084, doi:10.5194/acp-10-10067-2010, 2010.

Beekmann, M., Kerschbaumer, A., Reimer, E., Stern, R., and Möller, D.: PM measurement campaign HOVERT in the Greater Berlin area: model evaluation with chemically specified particulate matter observations for a one year period, Atmos. Chem. Phys., 7, 55–68, doi:10.5194/acp-7-55-2007, 2007.

Bessagnet, B., Hodzic, A., Vautard, R., Beekmann, M., Cheinet, S., Honoré, C., Liousse, C., Rouil, L.: Aerosol modeling with CHIMERE-preliminary evaluation at the continental scale, Atmos. Environ., 38, 2803–2817, 2004.

Bessagnet, B., Hodzic, A., Blanchard, O., Lattuati, M., Le Bihan, O., Marfaing, H., and Rouil, L.: Origin of particulate matter pollution episodes in wintertime over the Paris basin, Atmos. Environ., 39, 6159–6174, 2005.

Bessagnet, B., Menut, L., Curci, G., Hodzic, A., Guillaume, B., Liousse, C., Moukhtar, S., Pun, B., Seigneur C., and Schulz, M.: Regional modeling of carbonaceous aerosols over Europe – focus on secondary organic aerosols, J. Atmos. Chem., 61, 175–202, 2008.

Chazette, P.: The monsoon aerosol extinction properties at Goa during INDOEX as measured with lidar, J. Geophys. Res., 108, 4187, doi:10.1029/2002JD002074, 2003.

Chazette, P., Randriamiarisoa, H., Sanak, J., Couvert P., and Flamant, C.: Optical properties of urban aerosol from airborne and ground-based in situ measurements performed during the ESQUIF program, J. Geophys. Res, 110(D2), D02206, doi:10.1029/2004JD004810, 2005.

Chazette, P., Sanak., J., and Dulac, F.: New Approach for Aerosol Profiling with a Lidar Onboard an Ultralight Aircraft: Application to the African Monsoon Multidisciplinary Analysis, Environ. Sci. Technol., 41, 8335–8341, 2007.

Chazette, P., Raut, J.-C., Dulac, F., Berthier, S., Kim, S.-W., Royer, P., Sanak, J., Loaëc, S.

ACPD
11, 11861–11909, 2011

and Grigaut-Desbrosses, H.: Simultaneous observations of lower tropospheric continental aerosols with a ground-based, an airborne, and the spaceborne CALIOP lidar system, J. Geophys. Res., 115, D00H31, doi:10.1029/2009JD012341, 2010.
Debry, E., Fahey, K., Sartelet, K., Sportisse, B., and Tombette, M.: Technical Note: A new SIze REsolved Aerosol Model (SIREAM), Atmos. Chem. Phys., 7, 1537–1547, doi:10.5194/acp-7-1537-2007, 2007.
Deguillaume, L., Beekmann, M., and Menut, L.: Bayesian Monte Carlo analysis applied to regional scale inverse emission modelling for reactive trace gases, J. Geophys. Res., 112, D02307, doi:10.1029/2006JD007518, 2007.
Deguillaume, L., Beekmann, M., and Derognat, C.: Uncertainty evaluation of ozone production and its sensitivity to emission changes over the Ile-de-France region during summer periods, J. Geophys. Res., 113, D02304, doi:10.1029/2007JD009081, 2008.
De Moore, W. B., Sandetr, S. P., Golden, D. M., Hampton, R. F., Kurylo, M. J., Howard, C. J., Ravishankara, A. R., Kolb, C. E., and Molina, M. J.: Chemicla kinetics and photochemical data for use in stratospheric modeling evaluation, JPL publication, 94, 26, JPL, Pasadena, US, 1994.
Derognat, C., Beekmann, M., Bäumle, M., Martin, D., and Schmidt, H.: Effect of biogenic VOC emissions on the tropospheric chemistry during elevated ozone periods in Ile de France, J. Geophys. Res., 108, 8560, doi:10.1029/2001JD001421, 2003.
Dockery, D. and Pope, A.: Epidemiology of acute health effects: summary of time-series, in: Particles in Our Air: Concentration and Health Effects, edited by: Wilson, R. and Spengler, J. D., Harvard University Press, Cambridge, MA, USA, 123–147, 1996.
Dudhia J.: A nonhydrostatic version of the Penn state NCAR mesoscale model – validation tests and simulation of an atlantic cyclone and cold-front, Mon. Weather Rev., 121(5), 1493–1513, 1993.
Elias, T., Haeffelin, M., Drobinski, P., Gomes, L., Rangognio, J., Bergot, T., Chazette, P., Raut, J.-C., and Coulomb, M.: Particulate contribution to extinction of visible radiation: pollution, haze, and fog, Atmos. Res., 92(4), 443–454, doi:10.1016/j.atmosres.2009.01.006, 2009.
Fahey, K. M. and Pandis, S. N.: Optimizing model performance: variable size resolution in cloud chemistry modeling, Atmos. Environ., 35, 4471–4478, 2001.
Giannakaki, E., Balis, D. S., Amiridis, V., and Zerefos, C.: Optical properties of different aerosol types: seven years of combined Raman-elastic backscatter lidar measurements in Thessaloniki, Greece, Atmos. Meas. Tech., 3, 569–578, doi:10.5194/amt-3-569-2010, 2010.

ACPD
11, 11861–11909, 2011

Guenther, A., Karl, T., Harley, P., Wiedinmyer, C., Palmer, P. I., and Geron, C.: Estimates of global terrestrial isoprene emissions using MEGAN (Model of Emissions of Gases and Aerosols from Nature), Atmos. Chem. Phys., 6, 3181–3210, doi:10.5194/acp-6-3181-2006, 2006.

Gurjar, B. R., Butler, T. M., Lawrence, M. G., and Lelieveld, J.: Evaluation of Emissions and Air Quality in Megacities, Atmos. Environ., 42(7), 1593–1606, doi:10.1016/j.atmosenv.2007.10.048, 2008.

Haeffelin, M., Bergot, T., Elias, T., Tardif, R., Carrer, D., Chazette, P., Colomb, M., Drobinski, P., Dupont, E., Dupont, J.-C., Gomes, L., Musson-Genon, L., Pietras, C., Plana-Fattori, A., Protat, A., Rangognio, J., Raut, J.-C., Rémy, S., Richard, D., Sciare, J., and Zhang, X.: ParisFog, shedding new light on fog physical processes, B. Am. Meteorol. Soc., 91, 767–783, doi:10.1175/2009BAMS2671.1, 2010.

Hänel, G.: The properties of atmospheric aerosol particles as functions of the Relative humidity at thermodynamic equilibrium with the surrounding moist air, Adv. Geophys., 19, 73–188, 1976.

Hauglustaine, D. A., Hourdin, F., Jourdain, L., Filiberti, M.-A., Walters, S., Lamarque, J.-F., and Holland, E. A.: Interactive chemistry in the Laboratoire de Météorologie Dynamique general circulation model: Description and background tropospheric chemistry evaluation, J. Geophys. Res., 109, D04314, doi:10.1029/2003JD003957, 2004.

Hodzic, A., Chepfer, H., Chazette, P., Beekmann, M., Bessagnet, B., Drobinski, P., Goloub, P., Haeffelin, M., Morille, Y., and Vautard, R.: Comparison of aerosol chemistry-transport model simulations with lidar and sun-photometer observations at a site near Paris, J. Geophys. Res., D23201, doi:10.1029/2004JD004735, 2004.

Hodzic A., Vautard, R., Bessagnet, B., Lattuati, M., Moreto, F.: Long-term urban aerosol simulation versus routine particulate matter observations, Atmos. Environ., 39, 5851–5864, 2005.

Holben, B. N., Eck, T. F., Slutsker, I., Tanré, D., Buis, J. P., Setzer, A., Vermote, E., Reagan, J. A., Kaufman, Y., Nakajima, T., Lavenu, F., Jankowiak, I., and Smirnov, A.: AERONET – A federated instrument network and data archive for aerosol characterization., Remote Sens. Environ., 66, 1–16, 1998.

Honoré, C., Rouïl, L., Vautard, R., Beekmann, M., Bessagnet, B., Dufour, A., Elichegaray, C., Flaud, J.-M., Malherbe, L., Meleux, F., Menut, L., Martin, D., Peuch, A., Peuch, V. H., and Poisson, N.: Predictability of European air quality: The assessment of three years of operational forecasts and analyses by the PREV'AIR system, J. Geophys. Res., 113, D04301,

ACPD
11, 11861–11909, 2011

doi:10.1029/2007JD008761, 2008.
Jacob, D. J.: Heterogeneous chemistry and tropospheric ozone, Atmos. Environ, 34, 2131–2159, 2000.
Klett, J. D.: Lidar inversion with variable backscatter/extinction ratios, Appl. Optics, 24, 1638–1643, 1985.
Kim, Y., Couvidat, F., Sartelet, K., and Seigneur, C.: Comparison of different gas-phase mechanisms and aerosol modules for simulating particulate matter formation, J. Air Waste Manage. Assoc., in press, 2011a.
Kim, Y., Sartelet, K., and Seigneur, C.: Formation of secondary aerosols over Europe: comparison of two gas-phase chemical mechanisms, Atmos. Chem. Phys., 11, 583–598, doi:10.5194/acp-11-583-2011, 2011b.
Konovalov, I. B., Beekmann, M., Richter, A., and Burrows, J. P.: Inverse modelling of the spatial distribution of NO_x emissions on a continental scale using satellite data, Atmos. Chem. Phys., 6, 1747–1770, doi:10.5194/acp-6-1747-2006, 2006.
Lavigne, C., Roblin, A., Chervet, P., and Chazette, P.: Experimental and theoretical studies of the aureole about a point source that is due to atmospheric scattering in the middle ultraviolet, Appl. Optics, 44, 1250–1262, 2005.
Lauwerys, R. R.: Toxicologie industrielle et intoxications professionnelles, Masson, 1982.
Lawrence, M. G., Butler, T. M., Steinkamp, J., Gurjar, B. R., and Lelieveld, J.: Regional pollution potentials of megacities and other major population centers, Atmos. Chem. Phys., 7, 3969–3987, doi:10.5194/acp-7-3969-2007, 2007.
Nenes, A., Pilinis, C., and Pandis, S.: ISORROPIA: A new thermodynamic equilibrium model for multicomponent inorganic aerosols, Aquat. Geochem., 4, 123–152, 1998.
Patashnik, H. and Rupprecht, E. G.: Continuous PM10 measurements using a tapered element oscillating microbalance, J. Air Waste Manag. Assoc., 41, 1079–1083, 1991.
Pun, B. K., Griffin, R. J., Seigneur, C., and Seinfeld, J. H.: Secondary organic aerosol 2. Thermodynamic model for gas/particle partitioning of molecular constituents, J. Geophys. Res., 107(D17), 4333, doi:10.1029/2001JD000542, 2002.
Pun, B., Seigneur, C., and Lohman, K.: Modeling secondary organic aerosol via multiphase partitioning with molecular data, Environ. Sci. Technol., 40, 4722–4731, 2006.
Randriamiarisoa, H., Chazette, P., Couvert, P., Sanak, J., and Mégie, G.: Relative humidity impact on aerosol parameters in a Paris suburban area, Atmos. Chem. Phys., 6, 1389–1407, doi:10.5194/acp-6-1389-2006, 2006.

ACPD
11, 11861–11909, 2011

Raut, J.-C. and Chazette, P.: Retrieval of aerosol complex refractive index from a synergy between lidar, sunphotometer and in situ measurements during LISAIR experiment, Atmos. Chem. Phys., 7, 2797–2815, doi:10.5194/acp-7-2797-2007, 2007.

Raut, J.-C. and Chazette, P.: Vertical profiles of urban aerosol complex refractive index in the frame of ESQUIF airborne measurements, Atmos. Chem. Phys., 8, 901–919, doi:10.5194/acp-8-901-2008, 2008.

Raut, J.-C. and Chazette, P.: Assessment of vertically-resolved PM_{10} from mobile lidar observations, Atmos. Chem. Phys., 9, 8617–8638, doi:10.5194/acp-9-8617-2009, 2009.

Raut, J.-C., Chazette, P., and Fortain, A.: New approach using lidar measurements to characterize spatiotemporal aerosol mass distribution in an underground railway station in Paris, Atmos. Environ., 43, 575–583, doi:10.1016/j.atmosenv.2008.10.002, 2009a.

Raut, J.-C., Chazette, P., and Fortain, A., Link between aerosol optical, microphysical and chemical measurements in an underground railway station in Paris, Atmos. Environ., 43, 860–868, doi:10.1016/j.atmosenv.2008.10.002, 2009b.

Rouil, L., Honoré, C., Vautard, R., Beekman, M., Bessagnet, B., Malherbe, L., Meleux, F., Dufour, A., Elichegaray, C., Flaud, J.-M., Menut, L., Martin, D., Peuch, V.-H. and Poisson, N.: PREV'AIR : an operational forecasting and mapping system for air quality in Europe, B. Am. Meteorol. Soc., 90, 73–83, doi:10.1175/2008BAMS2390.1, 2009.

Roustan, Y., Sartelet, K. N., Tombette, M., Debry, É., and Sportisse, B.: Simulation of aerosols and gas-phase species over Europe with the POLYPHEMUS system. Part II: Model sensitivity analysis for 2001, Atmos. Environ., 41, 6116–6131, doi:10.1016/j.atmosenv.2010.07.005, 2010.

Roustan Y., Pausader M., and Seigneur, C.: Estimating the effect of on-road vehicle emission controls on future air quality in Paris, France, Atmos. Environ., doi:10.1016/j.atmosenv.2010.10.010, in press, 2011.

Royer, P., Chazette, P., Lardier, M., and Sauvage, L.: Aerosol content survey by mini N2-Raman lidar: Application to local and long-range transport aerosols, Atmospheric Environment, in press, 2010.

Sartelet, K., Debry, E., Fahey, K., Roustan, Y., Tombette, M., and Sportisse, B.: Simulation of aerosols and gas-phase species over Europe with the Polyphemus system. Part I: model-to-data comparison for 2001, Atmos. Environ., 41(29), 6116–6131, doi:10.1016/j.atmosenv.2007.04.024, 2007a.

Sartelet, K., Hayami, H., and Sportisse, B.: Dominant aerosol processes during high-pollution

ACPD
11, 11861–11909, 2011

episodes over Greater Tokyo, J. Geophys. Res., 112, D14214, doi:10.1029/2006JD007885, 2007b.
Sartelet, K., Hayami, H., and Sportisse, B.: MICS Asia Phase II Sensitivity to the aerosol module, Atmos. Environ., 42(15), 3562–3570, doi:10.1016/j.atmosenv.2007.03.05, 2008.
Schmidt, H., Derognat, C., Vautard, R., and Beekmann, M.: A comparison of simulated and observed ozone mixing ratios for summer of 1998 in western Europe, Atmos. Environ., 35, 6277–6297, 2001.
Sciare, J., d'Argouges, O., Zhang, Q. J., Sarda-Estève, R., Gaimoz, C., Gros, V., Beekmann, M., and Sanchez, O.: Comparison between simulated and observed chemical composition of fine aerosols in Paris (France) during springtime: contribution of regional versus continental emissions, Atmos. Chem. Phys., 10, 11987–12004, doi:10.5194/acp-10-11987-2010, 2010.
Seinfeld, J. H. and Pandis, S. N.: Atmospheric chemistry and physics: From air pollution to climate change, Wiley-Interscience, 1997.
Simpson, D., Winiwarter, W., Börjesson, G., Cinderby, S., Rerreiro, A., Guenther, A., Hewitt, C. N., Janson, R., Khalil, M. A. K., Owen, S., Pierce, T. E., Puxbaum, H., Shearer, M., Skiba, U., Steinbrecher, R., Tarrasón, L., and Öquist, M. G.: Inventorying emissions from nature in Europe, J. Geophys. Res., 104(D7), 8113–8152, doi:10.1029/98JD02747, 1999.
Stockwell, W. R., Kirchner, F., Kuhn, M., and Seefeld, S: A new mechanism for regional atmospheric chemistry modeling, J. Geophys. Res., 102(D22), 25847–25879, 1997.
Tombette, M. and Sportisse, B: Aerosol modeling at a regional scale: Model-to-data comparison and sensitivity analysis over Greater Paris, Atmos. Environ., 41(33), 6941–6950, 2007.
Tombette, M., Chazette, P., Sportisse, B., and Roustan, Y.: Simulation of aerosol optical properties over Europe with a 3-D size-resolved aerosol model: comparisons with AERONET data, Atmos. Chem. Phys., 8, 7115–7132, doi:10.5194/acp-8-7115-2008, 2008.
Troen, I. B. and Mahrt, L: A simple model of the atmospheric boundary layer; sensitivity to surface evaporation, Bound.-Layer Meteorol., 37, 129–148, 1986.
Vautard, R., Beekmann, M., Roux, J., and Gombert, D.: Validation of a hybrid forecasting system for the ozone concentrations over the Paris region, Atmos. Environ. 35, 2449–2461, 2001.
Vautard, R., Menut, L., Beekmann, M., Chazette, P., Flamant, P. H., Gombert, D., Guédalia, D., Kley, D., Lefebvre, M.-P., Martin, D., Mégie, G., Perros, P., and Toupance, G.: A synthesis of the Air Pollution Over the Paris Region (ESQUIF) field campaign, J. Geophys. Res., 108(D17), 8558, doi:10.1029/2003JD003380, 2003.

ACPD
11, 11861–11909, 2011

Yu, S., Eder, B., Dennis, R., Chu, A.-H., and Schwartz, S. H.: New unbiased symmetric metrics for evaluation of air quality models, Atmos. Sci. Lett., 7, 26–34, 2006.

ACPD
11, 11861–11909, 2011

Table 1. GBML technical characteristics.

Laser	Nd:YAG 20 Hz 16 mJ @ 355 nm
Pulse length	~ 6 ns
Reception diameter	150 mm
Full overlap	150–200 m
Detector	Photomultiplier tubes
Filter bandwidth (FWHM)	0.3 nm
Data acquisition system	PXI 100 MHz
Raw resolution along the line of sight	1.5m
Temporal resolution	20 s
Lidar head size	~ 65 × 35 × 18 cm
Lidar head and electronics weight	~ 40 kg
Power supply	4 batteries (12 V, 75 A/h)
Battery lifetime	~ 3 h 30 min

ACPD
11, 11861–11909, 2011

Table 2. Meteorological conditions (wind direction and velocity at ~250m, relative humidity at ~200 m, and maximum surface temperature), levels of pollution (and PM_{10} concentrations), mean AOD (and standard deviation) at 355 nm and mean LR (and standard deviation) observed during the 10 MD involving GBML during the MEGAPOLI summer experiment.

		meteorological conditions						
day	hour hh:mm (LT)	wind direction (°)	wind speed ($m\,s^{-1}$) at ~250 m	relative humidity (%) at ~200 m	T_{max} (°C)	levels of pollution (PM_{10})	AOD ± standard deviation	LR ± standard deviation (sr)
01	from 12:48 to 15:58	Northeast	3.3–3.6	45	30	High (40–90 $\mu g\,m^{-3}$)	0.51±0.13	50.4±9.3
02	from 13:01 to 16:00	East	1.0–2.3	48	32	High (30–70 $\mu g\,m^{-3}$)	0.70±0.10	54.7±18.4
04	from 16:49 to 19:24	West	0.9–1.7	44	28	Low (10–30 $\mu g\,m^{-3}$)	0.24±0.04	85.2±12.6
15	from 13:07 to 16:42	Southwest	7.7–8.7	41	26	low – moderate (20–40 $\mu g\,m^{-3}$)	–	–
16	from 13:03 to 16:31	South	3.7–5	44	31	low-moderate (25–35 $\mu g\,m^{-3}$)	0.24±0.03	35.7±14.6
20	from 14:27 to 17:59	West	4.4–5.2	49	25	Low (10–20 $\mu g\,m^{-3}$)	0.20±0.13	40.7±9.5
21	from 13:40 to 16:43	Southwest	8.2–9.8	42	31	low – moderate (20–40 $\mu g\,m^{-3}$)	–	–
26	from 14:42 to 17:30	South	3.5–4.4	41	27	low (10–20 $\mu g\,m^{-3}$)	0.16±0.03	50.9±10
28	from 15:05 to 19:17	Southwest	3.5–4.2	43	25	low (10–30 $\mu g\,m^{-3}$)	0.19±0.01	35.8±5.6
29	from 14:22 to 19:02	Southwest	5.5–7.1	44	28	low – moderate (20–40 $\mu g\,m^{-3}$)	–	–

ACPD
11, 11861–11909, 2011

Table 3. Comparison of air masses origin determined from backward trajectories in the month of July between 2005 and 2010, observed in July 2009 and observed in July 2009 for MD only.

Origin of air masses	July 2005–2010	July 2009	July 2009 (MD only)
Northeast	7%	3%	10%
East	9%	3%	10%
Southeast	3%	2%	0%
South	4%	5%	20%
Southwest	20%	21%	40%
West	41%	60%	20%
Northwest	12%	6%	0%
North	4%	0%	0%

ACPD
11, 11861–11909, 2011

Table 4. Main characteristics of POLYPEMUS platform and CHIMERE model.

	POLYPHEMUS	CHIMERE
Number of vertical levels	9 levels from ground to 12 000 m: 0, 40, 120, 300, 800, 1500, 2400, 3500, 6000, 12 000.	8 levels up to 5500 m: 40, 120, 250, 480, 850, 1600, 2900, 5500.
Nestings /horizontal resolution	– Europe (35–70° N ; 15° W–35° E) with 0.5°×0.5° resolution – France (41–52° N; 5° W–10° E) with 0.1°×0.1° resolution – Ile de France (47.9–50.1° N; 1.2° W–3.5° E) with 0.02°×0.02° resolution	– continental domain (35–57.5° N; 10.5° W–22.5° E) with 0.5°×0.5° resolution – regional domain (47.45–50.66° N; 0.35° W–4.41° E) with 3 km resolution
Climatology	Climatology (Mozart for gas and Gocart for aerosols)	Climatology (LMDz for gas and aerosols)
Meteorological data	MM5	GFS-MM5with two nested grids at 45 km (European domain) and 15 km (North-West Europe) forced by FNL final analysis data from NCAR
Emission inventories	Anthropogenic emissions: Airparif and EMEP where Airparif is not available. Biogenic emissions: as in Simpson et al. (1999)	Anthropogenic emissions: Airparif 2005 (gas in IdF) EMEP where Airparif is not available BC and OC from LA MEGAN for biogenic emissiosn
Emission height of volumic sources	EMEP: height varying profil which depends on snap categories AIRPARIF: volumic source emission height given by the inventory	EMEP: height varying profil which depends on snap categories AIRPARIF: volumic source emission height given by the inventory
Inorganic parametrization	ISORROPIA (Nenes, 1998), bulk equilibrium assumption between gas and particles	ISORROPIA (Nenes, 1998)
SOA formation	Mechnistic representation (SuperSorgam, Kim et al., 2011)	Pun et al. (2006); Bessagnet (2008)
Aqueous phase of PM	VSRM (Fahey and Pandis, 2001)	Seinfeld and Pandis (1997)
Computation of liquid water content	ISORROPIA	ISORROPIA
Gaseous chemistry	RACM	Melchior2
Heterogeneous reactions between gas and aerosol phases	Jacob (2000) with low values for probabilities	Jacob (2000) De Moore (1994) Aumont (2003)
Coagulation of particles	yes	yes
Size distribution of PM	5 sections between 0.01 µm and 10 µm	8 sections between 0.01 µm and 10 µm
Parameterization of the vertical diffusion coefficient	Troen and Mahrt (1986)	Troen and Mahrt (1986)

ACPD
11, 11861–11909, 2011

Table 5. Slope of the regression analysis (C_0), single scattering albedo ($\omega_{0,355}$) and Angstrom exponent (a) values used for the calculation of the specific extinction cross-section at 355 nm ($s_{ext,355}$) for urban, peri-urban and rural aerosol types. The uncertainties on the specific extinction cross-section and the total uncertainty on PM_{10} retrieval are also indicated for different AOD values.

Aerosol type	C_0 ($g\,m^{-2}$)	$\omega_{0,355}$	a	$s_{ext,355}$ ($m^2\,g^{-1}$)	Uncertainty on $s_{ext,355}$	Uncertainty on PM_{10} for different AOD		
						0.1	0.2	0.5
Urban	0.981	0.89	2.07	4.5	12 %	24%	17%	13%
Peri-urban	0.821	0.93	2.15	5.9	12 %	24%	17%	13%
Rural	0.386	0.91	1.36	7.1	26 %	33%	28%	26%
Dust	–	0.94	~0.8	1.1	26 %	33%	28%	26%

ACPD
11, 11861–11909, 2011

Table 6. Root Mean-Square Errors (RMSE) and Mean Absolute Percentage Error (MAPE) on PM_{10} calculated for each MD between GBML/POLYPHEMUS, GBML/CHIMERE, GBML/AIRPARIF, POLYPHEMUS/AIRPARIF and CHIMERE/AIRPARIF at ground level and ~250 m. The comparisons with GBML measurements have been made with rural, peri-urban and urban relationships. The expected uncertainties on GBML-derived PM_{10} have also been computed for rural, peri-urban and urban relationships taking into account AOD observed during each MD. Note that for the 15 July a mixing of dust and peri-urban relationships has been used in lidar inversion.

Day		Mean wet PM_{10} ± variability			Root Mean Square Error in µg m^{-3} (and Mean Absolute Percentage Error in %)					
					Ground level			~250 m		
Optical-to-mass relation-ships		Lidar	POLY-PHEMUS	CHIMERE	AIRPARIF/ Lidar	AIRPARIF/ POLY-PHEMUS	AIRPARIF/ CHIMERE	Lidar/ POLYPHEMUS	Lidar/ CHIMERE	Expected uncer-tainty on lidar PM_{10} (%)
01	Urban	55.3±23.2	45.5±16.3	32.8±10.0	19.2 (31.5%)	14.3 (26.6%)	14.5 (29.5%)	14.3 (19.9%)	26.9 (46.5%)	14%
	Peri-urban	43.0±18.0			4.9 (8.1%)			7.5 (13.4%)	14.2 (25.1%)	14%
	Rural	34.7±14.5			9.1 (14.8%)			12.6 (29.0%)	7.1 (17.2%)	27%
02	Urban	60.0±7.0	32.5±3.6	31.8±4.0	19.6 (38.5%)	16.4 (42.5%)	12.5 (26.8%)	28.7 (59.9%)	28.9 (61.1%)	13%
	Peri-urban	46.7±5.4			7.0 (14.4%)			15.7 (38.2%)	15.7 (38.0%)	13%
	Rural	37.6±4.4			5.9 (11.3%)			7.8 (19.5%)	7.4 (19.0%)	27%
04	Urban	24.0±2.4	11.9±2.7	13.9±5.3	6.2 (24.3%)	7.8 (48.6%)	7.6 (41.6%)	12.5 (67.9 %)	11.2 (58.1%)	17%
	Peri-urban	18.7±1.9			2.1 (10.0%)			7.4 (45.5%)	6.8 (40.4%)	17%
	Rural	15.1±1.5			4.0 (22.0 %)			4.3 (28.4%)	5.1 (26.8%)	29%
15	Urban	25.7±2.4	16.5±0.8	18.4±1.1	4.1 (11.4%)	7.8 (27.8%)	6.7 (22.2%)	9.5 (43.5%)	7.8 (32.9%)	18%
	Peri-urban	22.7±2.1			5.1 (16.3%)			6.6 (31.7%)	5.0 (21.2%)	18%
	Rural	20.7±2.0			6.5 (22.4%)			4.6 (22.7%)	3.3 (13.9%)	30%
16	Urban	25.3±3.4	22.7±2.2	14.7±2.4	4.9 (18.5%)	3.3 (11.2%)	9.6 (29.7%)	4.7 (15.6%)	11.3 (52.7%)	17%
	Peri-urban	19.7±2.6			8.8 (32.7%)			4.4 (16.6%)	6.0 (30.3%)	17%
	Rural	15.9±2.1			12.0 (53.0%)			7.4 (35.4%)	3.3 (15.7%)	29%
20	Urban	15.7±1.6	17.4±2.1	11.6±1.3	2.7 (13.0%)	1.3 (5.4%)	4.6 (28.4%)	2.8 (11.7%)	4.4 (30.1%)	18%
	Peri-urban	12.2±1.2			4.8 (29.1%)			5.6 (34.7%)	1.5 (10.6%)	18%
	Rural	9.9±1.0			7.0 (49.6%)			7.8 (55.0%)	2.2 (5.2%)	29%
21	Urban	33.7±4.0	20.7±1.8	20.8±3.5	6.9 (14.4%)	15.5 (40.1%)	15.6 (43.2%)	13.7 (47.3%)	13.5 (47.5%)	–
	Peri-urban	26.2±3.1			11.3 (26.8%)			6.5 (23.2%)	6.4 (23.3%)	–
	Rural	21.1±2.5			15.8 (44.7%)			2.9 (11.3%)	3.3 (11.8%)	–
26	Urban	18.2±1.3	8.1±1.1	8.8±1.9	3.6 (20.6%)	6.6 (51.4%)	4.5 (35.0%)	10.1 (76.7%)	9.5 (71.3%)	21%
	Peri-urban	14.2±1.0			1.3 (7.5%)			6.1 (54.3%)	5.5 (48.5%)	21%
	Rural	11.4±0.8			3.7 (25.7%)			3.4 (34.0%)	3.0 (28.7%)	31%
28	Urban	16.7±2.0	13.1±2.6	11.2±1.7	6.6 (35.1%)	5.9 (29.8%)	5.2 (27.5%)	4.4 (26.1%)	6.1 (40.1%)	18%
	Peri-urban	13.0±1.5			8.0 (43.0%)			2.5 (16.3%)	2.9 (19.8%)	18%
	Rural	10.5±1.2			9.7 (54.0%)			3.6 (23.5%)	2.1 (15.9%)	29%
29	Urban	26.9±3.2	11.3±1.8	11.0±1.6	13.1 (46.9%)	12.4 (41.9%)	13.3 (44.2%)	15.8 (82.5%)	16.1 (84.7%)	–
	Peri-urban	20.9±2.5			5.4(22%)			9.8 (60.6%)	10.1 (63.0%)	–
	Rural	16.9±2.0			0.3 (1.2%)			5.7 (40.6%)	6.0 (43.1%)	–
mean	Urban	30.2±5.0	20.0±3.5	17.5±3.3	8.7 (25.4%)	9.1 (32.5%)	9.4 (32.8%)	11.7 (45.1%)	13.6 (52.5%)	17%
	Peri-urban	22.7±3.9			5.9 (21.0%)			7.2 (33.4%)	7.4 (32.0%)	17%
	Rural	19.4±3.2			7.4 (29.9%)			6.0 (29.9%)	4.3 (19.7%)	29%

ACPD
11, 11861–11909, 2011

Table 7. Comparison of mean wet integrated PM_{10} between ground level up to 1 km a.g.l. for lidar with urban, peri-urban and rural parametrization, POLYPHEMUS and CHIMERE CTMs and RMSE and MAPE for integrated PM_{10} between GBML/POLYPHEMUS and BML/CHIMERE.

		Mean wet integrated PM_{10} ± variability			Root Mean Square Error on wet integrated PM_{10} in µg m^{-2} (and Mean Absolute Percentage Error in %)	
Day	Optical-to-mass relation-ships	Lidar	POLYPHEMUS	CHIMERE	Lidar/ POLYPHEMUS	Lidar/ CHIMERE
01	Urban	54.2±28.4	49.7±13.3	28.5±5.9	17.7 (24.6%)	34.6 (51.6%)
	Peri-urban	42.1±22.1			13.6 (31.7%)	21.6 (35.7%)
	Rural	34.0±17.8			17.6 (46.6%)	13.8 (31.4%)
02	Urban	57.0±10.0	37.8±3.8	30.8±4.1	22.1(44.0%)	27.8 (59.7%)
	Peri-urban	44.3±7.8			11.0 (22.2%)	15.4 (38.0%)
	Rural	35.7±6.3			7.8 (13.3%)	8.0 (20.5%)
04	Urban	19.5±3.5	12.4±2.8	13.2±5.0	8.3 (44.8%)	8.1 (44.6%)
	Peri-urban	15.2±2.7			4.6 (27.0%)	5.2 (28.7%)
	Rural	12.3±2.2			3.4 (21.8%)	4.8 (24.3%)
15	Urban	22.9±2.7	15.9±0.7	16.5±0.8	7.4 (35.1%)	7.1 (32.1%)
	Peri-urban	20.2±2.4			4.8 (23.3%)	4.7 (21.1%)
	Rural	18.4±2.2			3.2 (15.4%)	3.2 (14.9%)
16	Urban	22.2±3.8	22.0±2.0	13.7±2.0	3.9 (13.5%)	9.7 (46.9%)
	Peri-urban	17.3±3.0			5.7 (25.4%)	5.2 (25.3%)
	Rural	14.0±2.4			8.5 (45.2%)	3.2 (17.1%)
20	Urban	13.7±1.6	19.6±3.2	10.9±1.3	6.5 (34.5%)	3.2 (23.5%)
	Peri-urban	10.7±1.2			9.3 (58.2%)	1.4 (10.6%)
	Rural	8.6±1.0			11.3 (77.1%)	2.6 (23.5%)
21	Urban	25.5±4.2	21.2±1.7	19.4±3.3	6.3 (20.6%)	7.7 (27.8%)
	Peri-urban	19.8±3.2			4.0 (16.5%)	4.1 (15.1%)
	Rural	16.0±2.6			6.1 (30.0%)	5.0 (25.0%)
26	Urban	14.7±1.5	8.1±1.2	8.1±1.8	6.7 (58.2%)	6.7 (59.8%)
	Peri-urban	11.5±1.1			3.5 (34.5%)	3.5 (36.2%)
	Rural	9.3±0.9			1.4 (14.9%)	1.6 (18.2%)
28	Urban	13.7±2.3	13.0±2.4	10.6±1.4	2.6 (15.8%)	4.1 (27.3%)
	Peri-urban	10.6±1.8			3.3 (22.3%)	2.3 (17.3%)
	Rural	8.6±1.4			4.9 (40.5%)	2.8 (24.0%)
29	Urban	22.7±2.6	11.0±1.6	9.9±1.5	11.8 (69.1%)	12.9 (78.4%)
	Peri-urban	17.6±2.0			6.7 (46.1%)	7.8 (56.2%)
	Rural	14.2±1.7			3.4 (25.5%)	4.4 (36.0%)
mean	Urban	26.6±6.0	21.1±3.3	16.2±2.7	9.3 (36.0%)	12.2 (45.2%)
	Peri-urban	20.9±4.7			6.7 (30.7%)	7.1 (28.4%)
	Rural	17.1±3.9			6.8 (33.0%)	4.9 (23.5%)

ACPD
11, 11861–11909, 2011

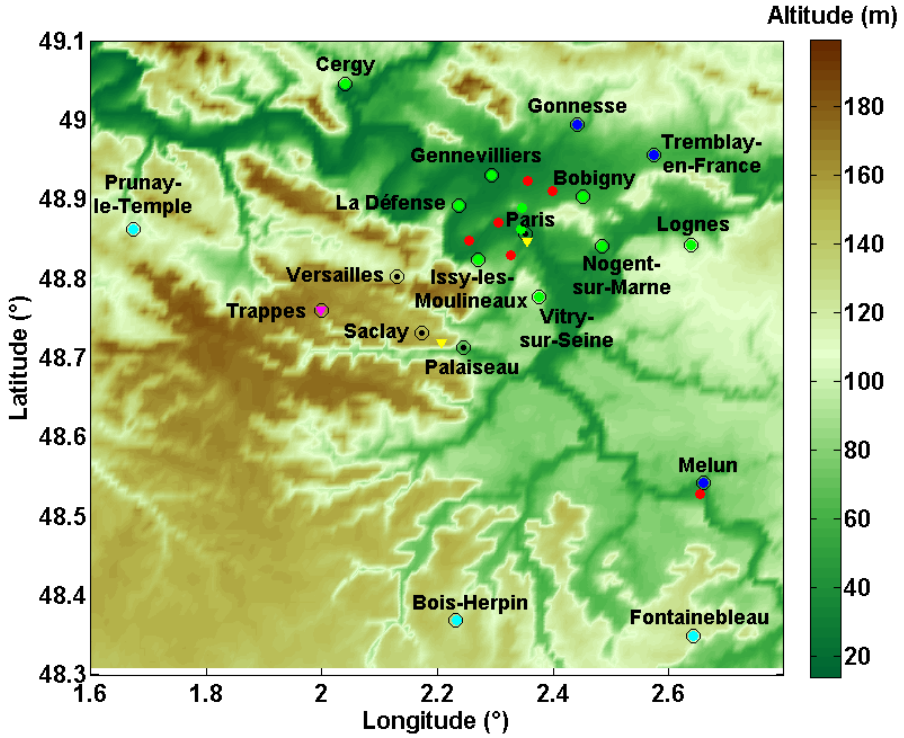

Fig. 1. Topographic map with the main cities in the vicinity of Paris. Colored circles indicate rural (in cyan), peri-urban (in blue), urban (in green) and traffic (in red) AIRPARIF stations measuring PM_{10}. Paris and Palaiseau AERONET sun-photometer stations and the location of Trappes radiosoundings are also indicated by yellow and pink triangles, respectively.

ACPD
11, 11861–11909, 2011

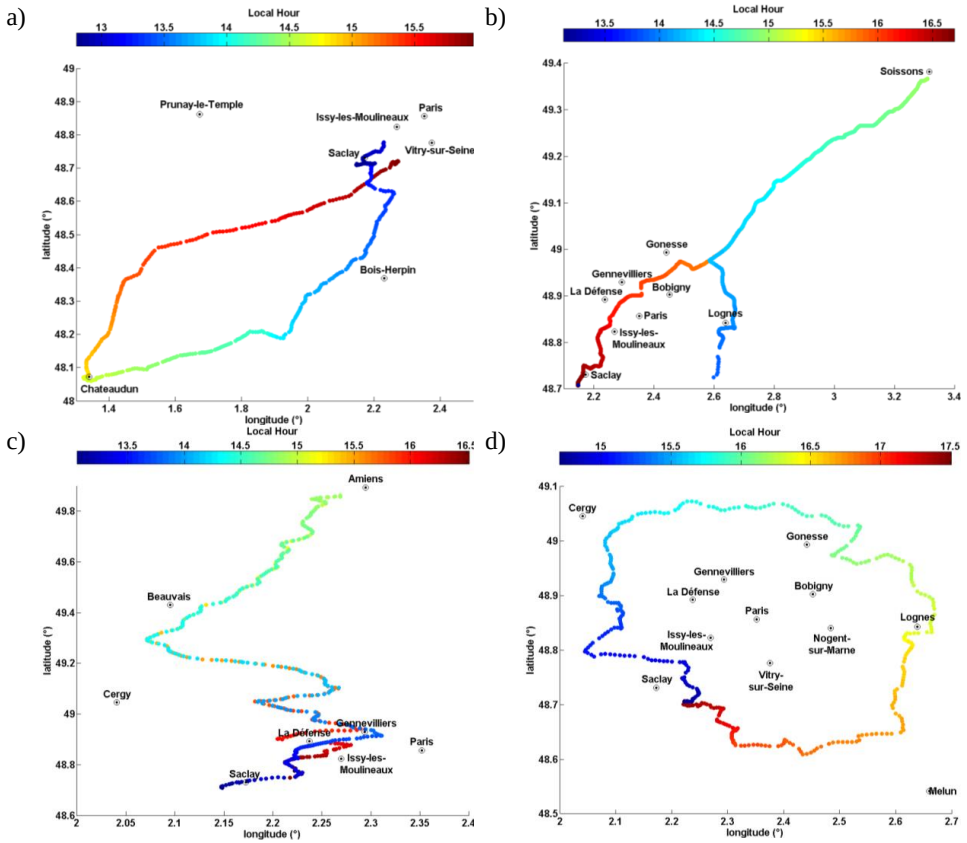

Fig. 2. Lidar van-circuits performed during the MEGAPOLI summer experiment for the 1 **(a)**, 15 **(b)**, 16 **(c)** and 26 **(d)** July 2009. The color scale indicates the decimal hours in LT.

ACPD
11, 11861–11909, 2011

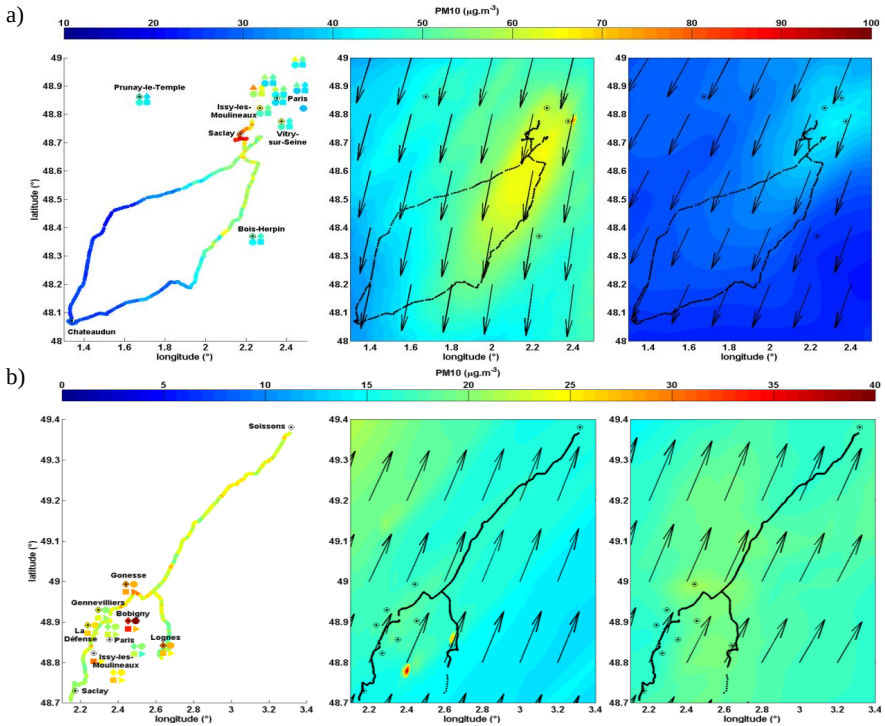

Fig. 3. Spatial distributions of wet PM_{10} at 12:00 h (UT) on 1 **(a)** and 15 **(b)** July derived from lidar measurements with the peri-urban relationship at 210 m (left column) and simulated at 12:00 h (UT) with the POLYPHEMUS model at 210 m (central column) and the CHIMERE model at 250 m (right column). Black arrows representing the wind at ~250 m used in POLYPHEMUS and CHIMERE simulations are shown on the central and right panels. Dry PM_{10} from AIRPARIF ground-based network are indicated by filled symbols at 13:00 h (up triangles), 1:00 4h (diamonds), 15:00 h (rounds), 16:00 h (squares), 17:00 h (right triangles), 18:00 h LT (pentagrams) in the left column. Note that for the 15 July a mixing of dust and peri-urban relationships has been used in lidar inversion.

ACPD
11, 11861–11909, 2011

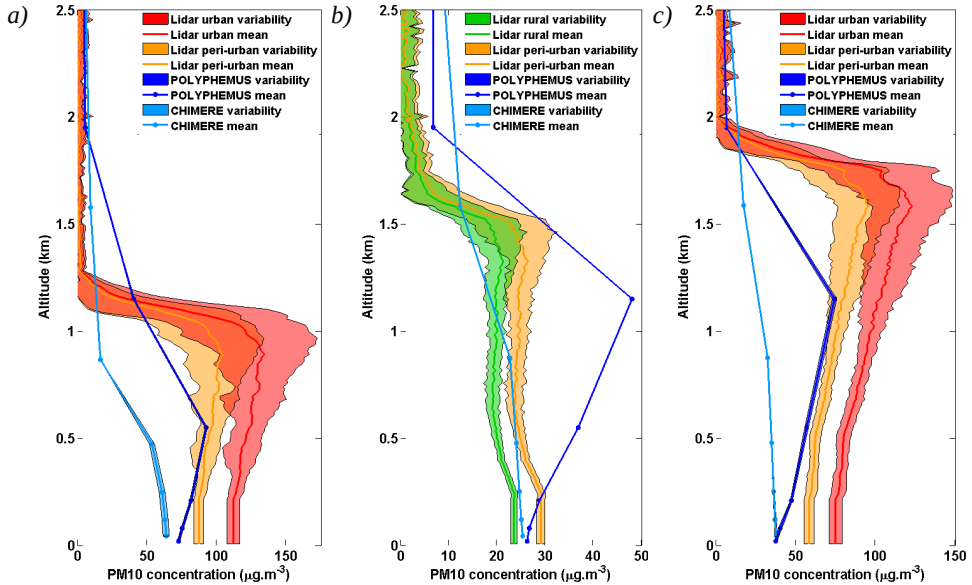

Fig. 4. Vertical profiles of PM_{10} concentrations on 1 July at the beginning of the van track near Saclay **(a)**, at Chateaudun **(b)** and at the end near Saclay **(c)**. The mean profile (solid line) and the variability observed over 20 profiles (shaded area) are indicated for the POLYPHEMUS plateform (dark blue), the CHIMERE model (light blue) and lidar with rural (green), peri-urban (orange) or urban relationships (red). Lidar measurements have been extended by a straight line under the full overlap height.

ACPD
11, 11861–11909, 2011

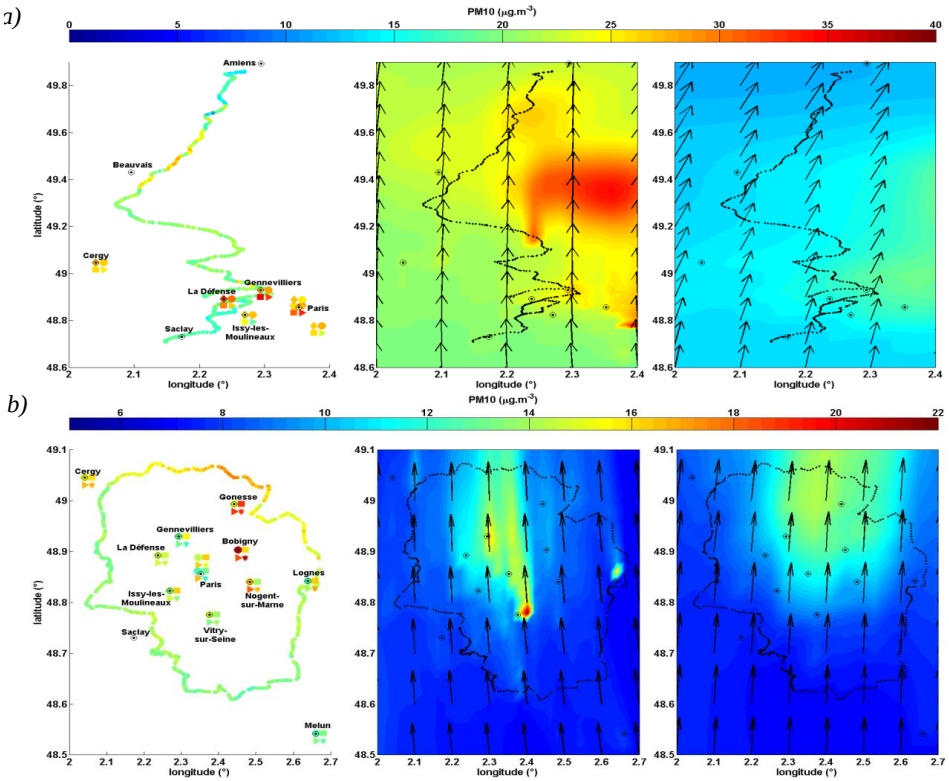

Fig. 5. Same as Fig. 3 on 16 **(a)** and 26 **(b)** July.

ACPD
11, 11861–11909, 2011

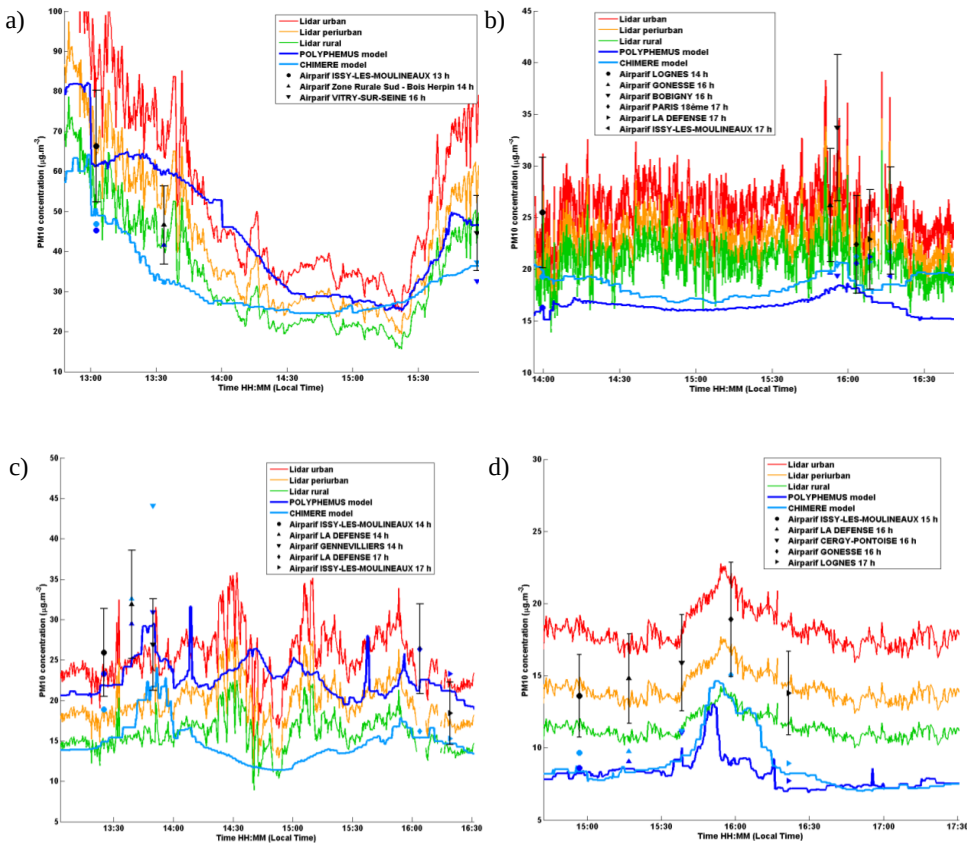

Fig. 6. Comparison for the 1 **(a)**, 15 **(b)**, 16 **(c)** and 26 **(d)** July of wet PM_{10} derived from GBML using urban (red curves), peri-urban (orange) and rural relationships (green) at 210 m, and wet PM_{10} extracted from POLYPHEMUS model at 210 m (in dark blue) and CHIMERE model at 250 m (in light blue). AIPARIF dry PM_{10} are indicated by black symbols for the nearest stations (located at less than 10 km from GBML) and dry PM_{10} modeled at the lowest level are indicated with dark blue (for POLYPHEMUS) and light blue (for CHIMERE) filled symbols. Note that for the 15 July a mixing of dust and pollution relationships has been used in lidar inversion.

ACPD
11, 11861–11909, 2011

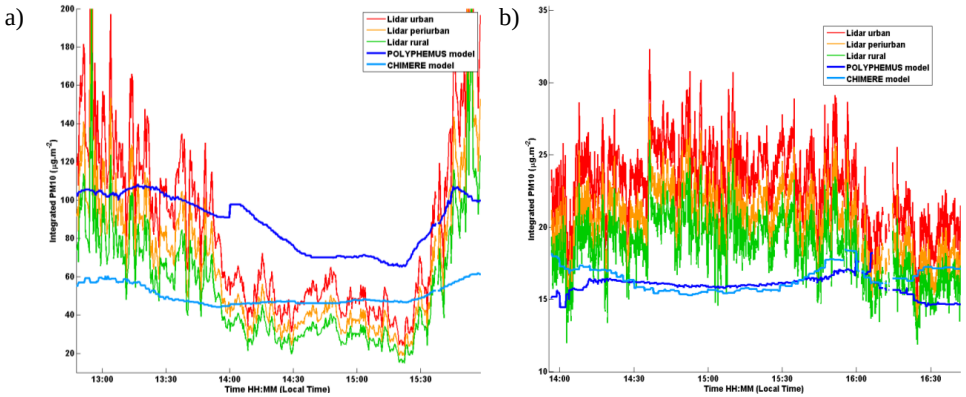

Fig. 7. Comparison for 1 **(a)** and 15 July 2009 **(b)** of wet integrated PM_{10} (between the ground and 1 km a.g.l.) derived from GBML using urban (red curves), peri-urban (orange) and rural relationships (green), and modeled with POLYPHEMUS plateform (in dark blue) and CHIMERE model (in light blue).

ACPD
11, 11861–11909, 2011